



TECH BRIEFS

NATIONAL AERONAUTICS AND SPACE ADMINISTRATION

-  **Technology Focus**
-  **Electronics/Computers**
-  **Software**
-  **Materials**
-  **Mechanics/Machinery**
-  **Manufacturing**
-  **Bio-Medical**
-  **Physical Sciences**
-  **Information Sciences**
-  **Books and Reports**

INTRODUCTION

Tech Briefs are short announcements of innovations originating from research and development activities of the National Aeronautics and Space Administration. They emphasize information considered likely to be transferable across industrial, regional, or disciplinary lines and are issued to encourage commercial application.

Availability of NASA Tech Briefs and TSPs

Requests for individual Tech Briefs or for Technical Support Packages (TSPs) announced herein should be addressed to

National Technology Transfer Center

Telephone No. (800) 678-6882 or via World Wide Web at www2.nttc.edu/leads/

Please reference the control numbers appearing at the end of each Tech Brief. Information on NASA's Innovative Partnerships Program (IPP), its documents, and services is also available at the same facility or on the World Wide Web at <http://ipp.nasa.gov>.

Innovative Partnerships Offices are located at NASA field centers to provide technology-transfer access to industrial users. Inquiries can be made by contacting NASA field centers listed below.

NASA Field Centers and Program Offices

Ames Research Center

Lisa L. Lockyer
(650) 604-1754
lisa.l.lockyer@nasa.gov

Dryden Flight Research Center

Gregory Poteat
(661) 276-3872
greg.poteat@dfrc.nasa.gov

Glenn Research Center

Kathy Needham
(216) 433-2802
kathleen.k.needham@nasa.gov

Goddard Space Flight Center

Nona Cheeks
(301) 286-5810
nona.k.cheeks@nasa.gov

Jet Propulsion Laboratory

Ken Wolfenbarger
(818) 354-3821
james.k.wolfenbarger@jpl.nasa.gov

Johnson Space Center

Michele Brekke
(281) 483-4614
michele.a.brekke@nasa.gov

Kennedy Space Center

David R. Makufka
(321) 867-6227
david.r.makufka@nasa.gov

Langley Research Center

Martin Waszak
(757) 864-4015
martin.r.waszak@nasa.gov

Marshall Space Flight Center

Jim Dowdy
(256) 544-7604
jim.dowdy@msfc.nasa.gov

Stennis Space Center

John Bailey
(228) 688-1660
john.w.bailey@nasa.gov

Carl Ray, Program Executive

Small Business Innovation
Research (SBIR) & Small
Business Technology
Transfer (STTR) Programs
(202) 358-4652
carl.g.ray@nasa.gov

Doug Comstock, Director

Innovative Partnerships
Program Office
(202) 358-2560
doug.comstock@nasa.gov



TECH BRIEFS

NATIONAL AERONAUTICS AND SPACE ADMINISTRATION



5 Technology Focus: Wireless Communications

- 5 Deployable Wireless Camera Penetrators
- 6 Hand-Held Units for Short-Range Wireless Biotelemetry
- 6 Wearable Wireless Telemetry System for Implantable BioMEMS Sensors
- 7 Electronic Escape Trails for Firefighters



9 Electronics/Computers

- 9 Architecture for a High-to-Medium-Voltage Power Converter
- 10 24-Way Radial Power Combiner/Divider for 31 to 36 GHz
- 10 Three-Stage InP Submillimeter-Wave MMIC Amplifier
- 11 Fast Electromechanical Switches Based on Carbon Nanotubes
- 12 Solid-State High-Temperature Power Cells
- 12 Fast Offset Laser Phase-Locking System



15 Manufacturing & Prototyping

- 15 Fabricating High-Resolution X-Ray Collimators
- 15 Embossed Teflon AF Laminate Membrane Microfluidic Diaphragm Valves



17 Mechanics/Machinery

- 17 Flipperons for Improved Aerodynamic Performance
- 18 System Estimates Radius of Curvature of a Segmented Mirror



19 Materials

- 19 Refractory Ceramic Foams for Novel Applications
- 20 Self-Deploying Trusses Containing Shape-Memory Polymers

- 21 Fuel-Cell Electrolytes Based on Organosilica Hybrid Proton Conductors

- 21 Molecules for Fluorescence Detection of Specific Chemicals



23 Bio-Medical

- 23 Cell-Detection Technique for Automated Patch Clamping
- 24 Redesigned Human Metabolic Simulator



27 Physical Sciences

- 27 Compact, Highly Stable Ion Atomic Clock
- 28 LiGa(OTf)₄ as an Electrolyte Salt for Li-Ion Cells
- 29 Compact Dielectric-Rod White-Light Delay Lines
- 29 Single-Mode WGM Resonators Fabricated by Diamond Turning
- 30 Mitigating Photon Jitter in Optical PPM Communication
- 31 MACOS Version 3.31
- 31 Fiber-Optic Determination of N₂, O₂, and Fuel Vapor in the Ullage of Liquid-Fuel Tanks



33 Information Sciences

- 33 Spiking Neurons for Analysis of Patterns
- 33 Symmetric Phase-Only Filtering in Particle-Image Velocimetry



35 Books & Reports

- 35 Efficient Coupler for a Bessel Beam Dispersive Element
- 35 Attitude and Translation Control of a Solar Sail Vehicle

This document was prepared under the sponsorship of the National Aeronautics and Space Administration. Neither the United States Government nor any person acting on behalf of the United States Government assumes any liability resulting from the use of the information contained in this document, or warrants that such use will be free from privately owned rights.



Deployable Wireless Camera Penetrators

Disposable, wireless camera darts can be used in zero G, or for surface surveys.

NASA's Jet Propulsion Laboratory, Pasadena, California

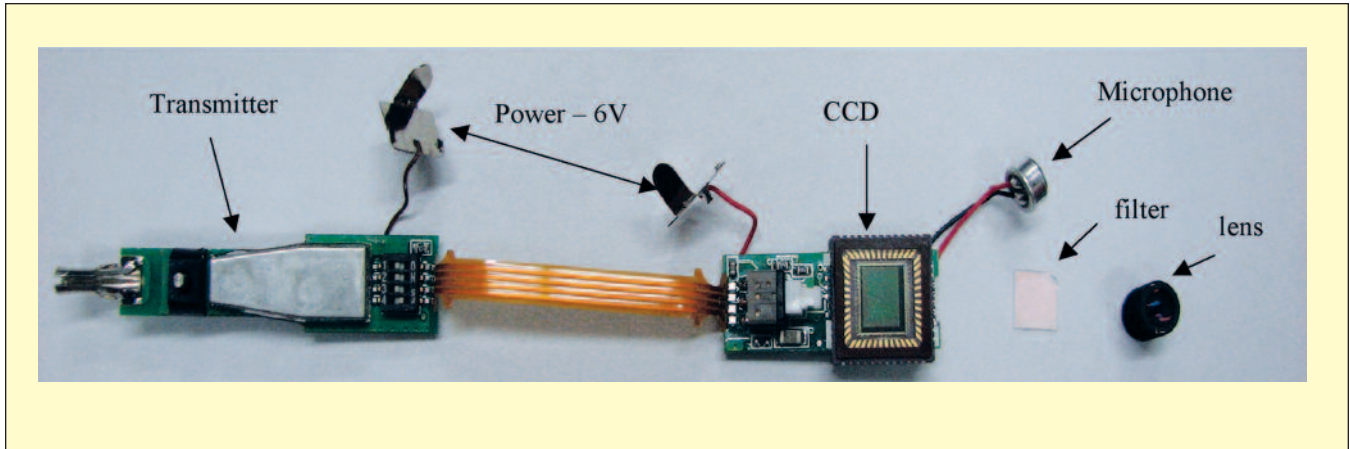


Figure 1. Components of a "Spy Pen" Camera incorporated into the dart camera weigh less than 8 grams. The unit produces VGA color images and sound at 30 frames per second and transmits up to 100 m.



Figure 2. CAD Models of the penetrator prototype.

A lightweight, low-power camera dart has been designed and tested for context imaging of sampling sites and ground surveys from an aerobot or an orbiting spacecraft in a microgravity environment. The camera penetrators also can be used to image any line-of-sight surface, such as cliff walls, that is difficult to access.

Tethered cameras to inspect the surfaces of planetary bodies use both power and signal transmission lines to operate. A tether adds the possibility of inadvertently anchoring the aerobot, and requires some form of station-keeping capability of the aerobot if extended examination time is required. The new camera penetrators are deployed without a tether, weigh less than 30 grams, and are disposable. They are designed to drop from any altitude with the boost in transmitting power currently demonstrated at approximately 100-m line-of-sight. The penetrators also can be deployed to monitor lander or rover operations from a distance, and can be used for surface surveys or for context information gathering from a touch-and-go sampling site.

Thanks to wireless operation, the complexity of the sampling or survey mechanisms may be reduced. The penetrators may be battery powered for short-duration missions, or have solar panels for longer or intermittent duration missions. The imaging device is embedded in the penetrator, which is dropped or

projected at the surface of a study site at 90° to the surface. Mirrors can be used in the design to image the ground or the horizon. Some of the camera features were tested using commercial "nanny" or "spy" camera components with the charge-coupled device (CCD) looking at a direction parallel to the ground.

Figure 1 shows components of one camera that weighs less than 8 g and occupies a volume of 11 cm³. This camera could transmit a standard television signal, including sound, up to 100 m.

Figure 2 shows the CAD models of a version of the penetrator. A low-volume array of such penetrator cameras could be deployed from an aerobot or a spacecraft onto a comet or asteroid. A system of 20 of these penetrators could be designed and built in a 1- to 2-kg mass envelope.

Possible future modifications of the camera penetrators, such as the addition of a chemical spray device, would allow the study of simple chemical reactions of reagents sprayed at the landing site and looking at the color changes. Zoom lenses also could be added for future use.

This work was done by Mircea Badescu, Jack Jones, Stewart Sherrit, and Jiunn Jenq Wu of Caltech for NASA's Jet Propulsion Laboratory. For more information, contact iaoffice@jpl.nasa.gov. NPO-44447

Hand-Held Units for Short-Range Wireless Biotelemetry

These units would power surgically implanted sensors.

John H. Glenn Research Center, Cleveland, Ohio

Special-purpose hand-held radio-transceiver units have been proposed as means of short-range radio powering and interrogation of surgically implanted microelectromechanical sensors and actuators. These units are based partly on the same principles as those of the units described in "Printed Multi-Turn Loop Antennas for RF Biotelemetry" (LEW-17879-1), *NASA Tech Briefs*, Vol. 31, No. 6 (June 2007), page 48. Like the previously reported units, these units would make it unnecessary to have wire connections between the implanted devices and the external equipment used to activate and interrogate them.

Like a unit of the previously reported type, a unit of the type now proposed would include a printed-circuit antenna on a dielectric substrate. The antenna circuitry would include integrated surface-mount inductors for impedance tuning. Circuits for processing the signals transmitted and received by the antenna would be included on the substrate.

During operation, the unit would be positioned near (but not in electrical contact with) a human subject, in proximity to a microelectromechanical sensor or actuator that has been surgically implanted in the subject. It has been

demonstrated that significant electromagnetic coupling with an implanted device could be established at a distance of as much as 4 in. (≈ 10 cm). During operation in the interrogation mode, the antenna of the unit would receive a radio telemetry signal transmitted by the surgically implanted device.

The antenna substrate would have dimensions of approximately 3.25 by 3.75 inches (approximately 8.3 by 9.5 cm). The substrate would have a thickness of the order of 30 mils (of the order of a somewhat less than a millimeter). The substrate would be made of low-radio-frequency-loss dielectric material that could be, for example, fused quartz, alumina, or any of a number of commercially available radio-frequency dielectric composite materials. The antenna conductors would typically be made of copper or a combination of chromium and gold. The choice of metal and the thickness of the metal layer(s) would depend on the choice of substrate material. For example, on a quartz or alumina substrate, one would typically use a layer of chromium 150 Å thick and a layer of gold 2 μm thick.

The proposed units and the implanted devices that they would interrogate or ac-

tivate would be inherently safe to use. They would operate at low radiated-power levels for short interrogation times (typically, milliseconds). Hence, there would be little local heating of tissues surrounding the implanted devices and little absorption of radio energy by such sensitive body parts as the eyes and the brain.

Because the implanted devices would not depend on battery power and would be activated only during short interrogation intervals and would otherwise be in the "off" state most of the time, the useful lifetimes of the implanted devices would be greater than those of comparable battery-powered implanted devices. The compactness of the hand-held transceiver units would facilitate transport and storage and would facilitate self-diagnosis by patients able to handle the units while away from medical facilities.

This work was done by Félix A. Miranda and Rainee N. Simons of Glenn Research Center. Further information is contained in a TSP (see page 1).

Inquiries concerning rights for the commercial use of this invention should be addressed to NASA Glenn Research Center, Innovative Partnerships Office, Attn: Steve Fedor, Mail Stop 4-8, 21000 Brookpark Road, Cleveland, Ohio 44135. Refer to LEW-17483-1.

Wearable Wireless Telemetry System for Implantable BioMEMS Sensors

Physiological monitoring would entail minimal risk, discomfort, or restriction of mobility.

John H. Glenn Research Center, Cleveland, Ohio

Telemetry systems of a type that have been proposed for the monitoring of physiological functions in humans would include the following subsystems:

- Surgically implanted or ingested units that would comprise combinations of microelectromechanical systems (MEMS)-based sensors [bioMEMS sensors] and passive radio-frequency (RF) readout circuits that would include miniature loop antennas.
- Compact radio transceiver units integrated into external garments for wirelessly powering and interrogating the implanted or ingested units.

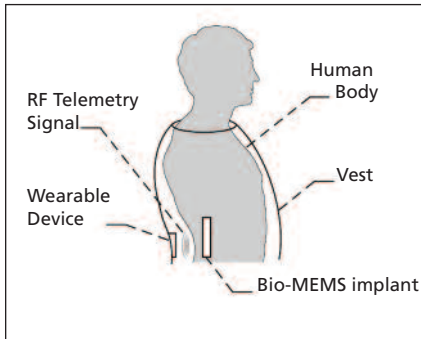
The basic principles of operation of

these systems are the same as those of the bioMEMS-sensor-unit/external-RF-powering-and-interrogating-unit systems described in "Printed Multi-Turn Loop Antennas for Biotelemetry" (LEW-17879-1) *NASA Tech Briefs*, Vol. 31, No. 6 (June 2007), page 48, and in the immediately preceding article, "Hand-Held Units for Short-Range Wireless Biotelemetry" (LEW-17483-1). The differences between what is reported here and what was reported in the cited prior articles lie in proposed design features and a proposed mode of operation.

In a specific system of the type now

proposed, the sensor unit would comprise mainly a capacitive MEMS pressure sensor located in the annular region of a loop antenna (more specifically, a square spiral inductor/antenna), all fabricated as an integral unit on a high-resistivity silicon chip. The capacitor electrodes, the spiral inductor/antenna, and the conductor lines interconnecting them would all be made of gold. The dimensions of the sensor unit have been estimated to be about 1x1x0.4 mm.

The external garment-mounted powering/interrogating unit would include a multi-turn loop antenna and signal-pro-



Relative location of the **Bio-MEMS** implantable sensor and the garment integrated wearable device.

cessing circuits. During operation, this external unit would be positioned in proximity to the implanted or ingested unit to provide for near-field, inductive coupling between the loop antennas, which we have as the primary and secondary windings of an electrical transformer.

In the first of two parts of an operational sequence, the loop antenna in the sensor unit would receive a pulse of RF energy transmitted via the loop antenna in the external powering/interrogating unit. This pulse would charge the capacitor in the pressure sensor and thereby

excite decaying oscillations in the resonant circuit constituted by the sensor capacitance and the loop inductance. In the second part of the operational sequence, some of the power of the decaying oscillations would be coupled from the loop in the sensor unit to the loop in the interrogating unit. The frequency of the decaying oscillation would be the resonance frequency, which would vary with the sensor capacitance and, hence, with the sensed pressure. Therefore, the frequency of the signal received by the external unit during the second part of the operational sequence would be measured, and any change in the frequency from a previous value would be taken as an indication of a change in pressure.

The proposed system would offer several advantages over prior invasive physiological-monitoring sensor systems:

- The sensor materials (high-resistivity silicon and gold) would not react with body fluids.
- High-resistivity silicon would cause less attenuation of signals in comparison with other substrate materials.
- The multi-loop antenna in the external unit could be fabricated inexpensively as a printed circuit.

sively as a printed circuit.

- The inductive-powering scheme eliminates the need for a battery in or alongside the sensor unit, thereby reducing the potential for leakage of toxic material into the patient's body.
- Because the sensor circuit would operate only when interrogated by the external unit, power dissipation in the patient and the consequent local heating and discomfort would be minimized and the operational lifetime of the sensor unit would be extended.
- Feed-through wires for power and telemetry, used in some other systems, would be eliminated, thereby greatly enhancing the patient's mobility and reducing the risk of infection.

This work was done by Rainee N. Simons, Félix A. Miranda, and Jeffrey D. Wilson of Glenn Research Center and Renita E. Simons of John Carroll University. Further information is contained in a TSP (see page 1).

Inquiries concerning rights for the commercial use of this invention should be addressed to NASA Glenn Research Center, Innovative Partnerships Office, Attn: Steve Fedor, Mail Stop 4-8, 21000 Brookpark Road, Cleveland, Ohio 44135. Refer to LEW-18222-1.

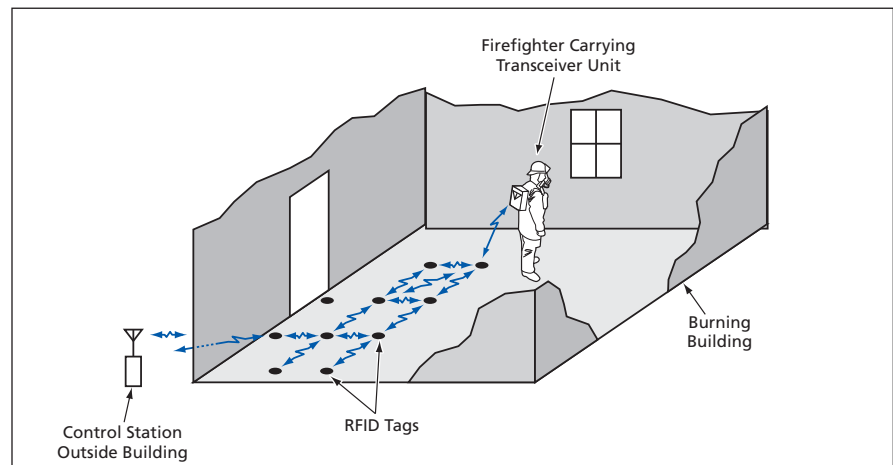
Electronic Escape Trails for Firefighters

Routes would be traced among RFID tags equipped with sensors showing temperatures.

Ames Research Center, Moffett Field, California

A proposed wireless-communication and data-processing system would exploit recent advances in radio-frequency identification devices (RFIDs) and software to establish information lifelines between firefighters in a burning building and a fire chief at a control station near but outside the building. The system would enable identification of trails that firefighters and others could follow to escape from the building, including identification of new trails should previously established trails become blocked.

The system would include a transceiver unit and a computer at the control station, portable transceiver units carried by the firefighters in the building, and RFID tags that the firefighters would place at multiple locations as they move into and through the building (see figure). Each RFID tag, having a size of the order of a few centimeters, would include at least standard RFID circuitry and possibly sensors for measuring such other relevant environmen-



RFID Tags would be dropped by a firefighter at numerous locations while moving through a burning building. The tags would serve as waypoint marks that would be interrogated by an RFID transceiver unit carried by the firefighter. The RFID tags would also relay sensory and position data to the control station outside the building

tal parameters as temperature, levels of light and sound, concentration of oxygen, concentrations of hazardous chemicals in smoke, and/or levels of nuclear

radiation. The RFID tags would be activated and interrogated by the firefighters' and control-station transceivers. Preferably, RFID tags would be config-

ured to communicate with each other and with the firefighters' units and the control station in an ordered sequence, with built-in redundancy.

In a typical scenario, as firefighters moved through a building, they would scatter many RFID tags into smoke-obscured areas by use of a compressed-air gun. Alternatively or in addition, they would mark escape trails by dropping RFID tags at such points of interest as mantraps, hot spots, and trail waypoints. The RFID tags could be of different types, operating at different frequencies to identify their functions, and possibly responding by emitting audible beeps when activated by signals transmitted by transceiver units carried by nearby firefighters.

It would be necessary to distribute the RFID tags densely enough to ensure reliable communication. A typical RFID of a type now commercially available is a passive device that operates at a carrier frequency of about 433 MHz, and can communicate with another such RFID, using one of several standard serial digital-data-communication proto-

cols, over a distance of as much as about 7 m. In the proposed system, supplementary units could be dispersed along with the RFID tags to increase signal power sufficiently to ensure communication with firefighter's transceiver units and/or with the control station, which would otherwise be out of range.

In a typical application of a basic version of the system, inexpensive RFID tags having limited range would be dispersed densely enough to enable a firefighter to go from one waypoint to another. The tags could include temperature sensors to alert firefighters to dangerously hot waypoints. If more than one tag were dropped within communication range, a tag indicating a safe temperature could become an alternate waypoint for a route out of the building.

In a more advanced version of the system, the RFID tags could communicate with each other via local daisy chains, relaying data on hot spots to the fire chief at the control station. The dispersed RFID tags could also constitute elements of an indirect positioning system.

If the system were designed to measure signal-propagation delays among the various tags and firefighters' transceivers, then the relative positions of the tags and the firefighters could be computed from these delays. The software for computing the relative positions could be integrated into a more comprehensive computer program that would correlate the positions with a three-dimensional map or graphical display of the building. In that case, locations of firefighters, hot spots, and mantraps, could all be presented on a single building display that would assist the fire chief in planning safe escape routes.

This work was done by Charles Jorgensen and John Schipper of Ames Research Center and Bradley Betts of Computer Science Corp.

This invention is owned by NASA and a patent application has been filed. Inquiries concerning rights for the commercial use of this invention should be addressed to the Ames Technology Partnerships Division at (650) 604-2954. Refer to ARC-15487-1.



Architecture for a High-to-Medium-Voltage Power Converter

High input voltage would be divided evenly among many converter blocks.

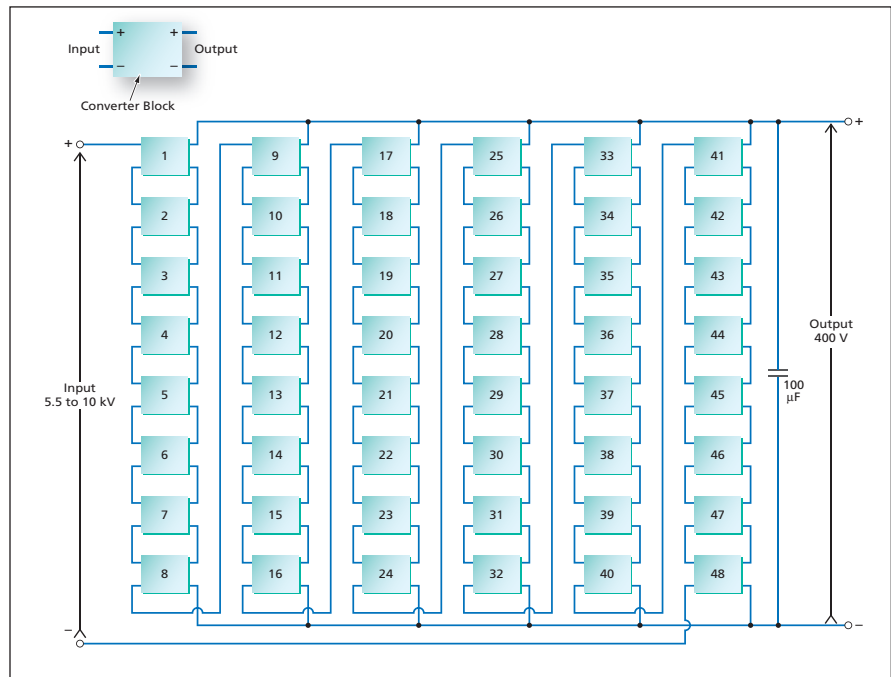
NASA's Jet Propulsion Laboratory, Pasadena, California

A power converter now undergoing development is required to operate at a DC input potential ranging between 5.5 and 10 kV and a DC output potential of 400 V at a current up to 25 A. This power converter is also required to be sufficiently compact and reliable to fit and operate within the confines of a high-pressure case to be lowered to several miles (≈ 5 km) below the surface of the ocean. The architecture chosen to satisfy these requirements calls for a series/parallel arrangement of 48 high-frequency, pulse-width-modulation (PWM), transformer-isolation DC-to-DC power converter blocks.

The input sides of the converter blocks would be connected in series so that the input potential would be divided among them, each of them being exposed to an input potential of no more than 10 kV/48 ≈ 210 V. The series connection of inputs would also enforce a requirement that all the converter blocks operate at the same input current. The outputs of the converter blocks would be connected in a matrix comprising 6 parallel legs, each leg being a cascade of eight outputs wired in series (see figure).

All the converter blocks would be identical within the tolerances of the values of their components. A single voltage feedback loop would regulate the output potential. All the converter blocks would be driven by the same PWM waveform generated by this feedback loop. The power transformer of each converter block would have a unity turns ratio and would be capable of withstanding as much as 10 kVDC between its primary and secondary windings. (Although, in general, the turns ratio could be different from unity, the simplest construction for minimizing leakage and maximizing breakdown voltage is attained at a turns ratio of unity.)

Each converter block would contain an output filter that would serve two purposes, one being the conventional purpose of smoothing out the pulsations in the output potential. The other purpose is to interact with the power transformer in such a manner as to result in equal sharing



Converter Blocks would be connected in a series/parallel arrangement, which, together with control circuitry, would result in equal sharing of current and voltage.

of voltage among all the converter blocks.

The secondary-side circuits in the converter blocks would include synchronous rectifiers instead of diode rectifiers, in order to prevent inductor-current discontinuities at no load or light load. Such discontinuities could upset the desired sharing of voltage because they would cause the output potential to depend on the output current in addition to the PWM duty cycle.

The following two additional features would not be crucial to sharing of current and voltage but would be needed for good performance:

- Each converter block would include a two-stage input filter that would smooth out input-current pulsations caused by switching of the input voltage applied to the primary winding of the power transformer. The input filter would include damping resistors to prevent oscillations that could otherwise occur in the presence of negative-input resistance of the converter.
- The peak current in the switch on the

primary side of one of the converters blocks would be sensed and compared with an error signal after the addition of an external ramp signal. This current feedback loop will improve the dynamic response and provide natural peak current limiting of the converter.

This work was done by Vatché Vorperian of Caltech for NASA's Jet Propulsion Laboratory. Further information is contained in a TSP (see page 1).

In accordance with Public Law 96-517, the contractor has elected to retain title to this invention. Inquiries concerning rights for its commercial use should be addressed to:

*Innovative Technology Assets Management
JPL*

*Mail Stop 202-233
4800 Oak Grove Drive
Pasadena, CA 91109-8099
(818) 354-2240*

E-mail: iaoffice@jpl.nasa.gov

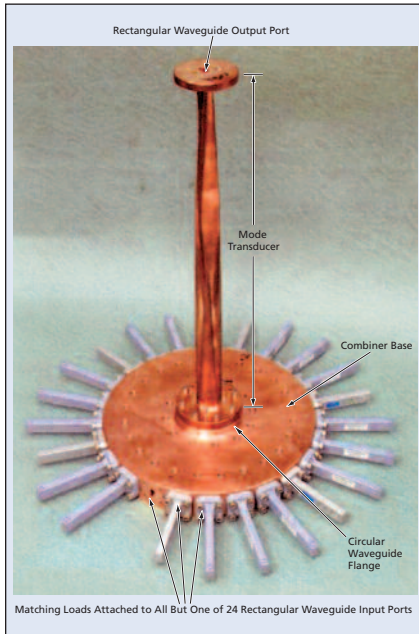
Refer to NPO-40364, volume and number of this NASA Tech Briefs issue, and the page number.

24-Way Radial Power Combiner/Divider for 31 to 36 GHz

A unique design affords high bandwidth with high order of combining.

NASA's Jet Propulsion Laboratory, Pasadena, California

The figure shows a prototype radial power-combining waveguide structure, capable of operation at frequencies from 31 to 36 GHz, that features an unusually large number ($N = 24$) of combining (input) ports. The combination of wide-band operation and large N is



This Power Combiner contains 24 internal reduced-height radial waveguides with impedance-transforming height and width steps, plus an internal central matching post.

achieved by incorporating several enhancements over a basic radial power-combiner design. In addition, the structure can be operated as a power divider by reversing the roles of the input and output ports.

In this structure, full-height waveguides at the combining ports are matched in impedance to reduced-height radial waveguides inside the combiner base. This match is effected by impedance-transforming stepped waveguide sections. This matching scheme is essential to achievement of large N because N is limited by the height of the waveguides in the base.

Power is coupled from the 24 reduced-height radial waveguides into the TE_{01} mode of a circular waveguide in the base with the help of a matching post at the bottom of the base. ("TE" signifies "transverse electric," the first subscript is the azimuthal mode number, and the second subscript is the radial mode number.) More specifically, the matching post matches the reflections from the walls of the 24 reduced-height waveguides and enables the base design to exceed the bandwidth requirement.

After propagating along the circular waveguide, the combined power is coupled, via a mode transducer, to a rectangular waveguide output port. The mode

transducer is divided into three sections, each sized and shaped as part of an overall design to satisfy the mode-conversion and output-coupling requirements while enabling the circular waveguide to be wide enough for combining the 24 inputs over the frequency range of 31 to 36 GHz. During the design process, it was found that two different rectangular waveguide outputs could be accommodated through modification of only the first section of the mode converter, thereby enabling operation in multiple frequency ranges.

This work was done by Larry Epp, Daniel Hoppe, Abdur Khan, and Daniel Kelley of Caltech for NASA's Jet Propulsion Laboratory. Further information is contained in a TSP (see page 1).

In accordance with Public Law 96-517, the contractor has elected to retain title to this invention. Inquiries concerning rights for its commercial use should be addressed to:

Innovative Technology Assets Management
JPL

Mail Stop 202-233
4800 Oak Grove Drive
Pasadena, CA 91109-8099
(818) 354-2240

E-mail: iaoffice@jpl.nasa.gov

Refer to NPO-41511, volume and number of this NASA Tech Briefs issue, and the page number.

Three-Stage InP Submillimeter-Wave MMIC Amplifier

Submillimeter-wave amplifiers can enable more sensitive receivers for earth science, planetary remote sensing, and astrophysics telescopes.

NASA's Jet Propulsion Laboratory, Pasadena, California

A submillimeter-wave monolithic integrated-circuit (S-MMIC) amplifier has been designed and fabricated using an indium phosphide (InP) 35-nm gate-length high electron mobility transistor (HEMT) device, developed at Northrop Grumman Corporation. The HEMT device employs two fingers each 15 micrometers wide. The HEMT wafers are grown by molecular beam epitaxy (MBE) and make use of a pseudomorphic $In_{0.75}Ga_{0.25}As$ channel, a silicon delta-doping layer as the electron supply, an $In_{0.52}Al_{0.48}As$ buffer layer, and an InP substrate. The three-stage de-

sign uses coplanar waveguide topology with a very narrow ground-to-ground spacing of 14 micrometers. Quarter-wave matching transmission lines, on-chip metal-insulator-metal shunt capacitors, series thin-film resistors, and matching stubs were used in the design. Series resistors in the shunt branch arm provide the basic circuit stabilization. The S-MMIC amplifier was measured for S-parameters and found to be centered at 320 GHz with 13–15-dB gain from 300–345 GHz.

This chip was developed as part of the DARPA Submillimeter Wave Imag-

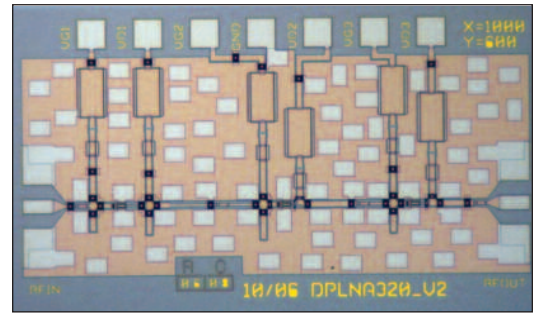
ing Focal Plane Technology (SWIFT) program (see figure). Submillimeter-wave amplifiers could enable more sensitive receivers for earth science, planetary remote sensing, and astrophysics telescopes, particularly in radio astronomy, both from the ground and in space. A small atmospheric window at 340 GHz exists and could enable ground-based observations. However, the submillimeter-wave regime (above 300 GHz) is best used for space telescopes as Earth's atmosphere attenuates most of the signal through water and oxygen absorption. Future radio

telescopes could make use of S-MMIC amplifiers for wideband, low noise, instantaneous frequency coverage, particularly in the case of heterodyne array receivers.

This work is aimed at pushing the MMIC and transistor technologies toward higher frequencies and, at these higher frequencies (>300 GHz), a wealth of spectral lines of molecular species exist and could be studied with more sensitive receivers. There are potential applications for future millimeter-wave Earth observational instruments such as the Scanning Microwave Limb Sounder, GeoSTAR, and other planetary instrument concepts being proposed, such as the Microwave Sounding Unit for Mars. These future

instruments and missions need high-gain, low-noise amplifiers at or above 180 GHz. Implementation of high-gain, low-noise amplifiers would greatly improve the signal-to-noise ratio of future heterodyne receivers.

This work was done by David Pukala, Lorene Samoska, King Man Fung, and Todd Gaier of Caltech and William Deal, Richard Lai, Gerry Mei, and Stella Makishi of Northrop Grumman Corporation for NASA's Jet Propulsion Laboratory. The contributors would like to acknowledge the support of Dr. Mark Rosker and the Army Research Laboratory. This work was supported by the DARPA SWIFT



A Chip Photograph of the 320-GHz three-stage S-MMIC amplifier.

Program and Army Research Laboratory under the DARPA MIPR no.06-U037 and ARL Contract no. W911QX-06-C-0050. Further information is contained in a TSP (see page 1). NPO-45046

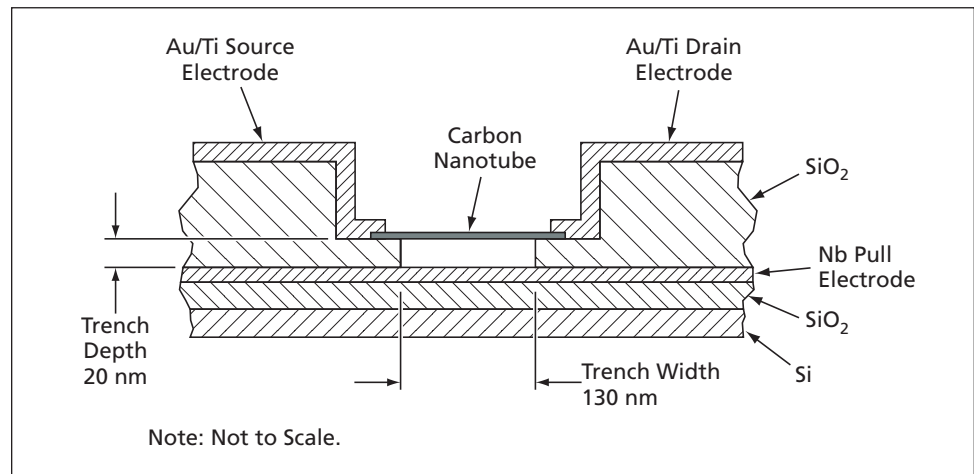
Fast Electromechanical Switches Based on Carbon Nanotubes

Potential applications include computer memory, cell phones, and scientific instruments.

NASA's Jet Propulsion Laboratory, Pasadena, California

Electrostatically actuated nano-electromechanical switches based on carbon nanotubes have been fabricated and tested in a continuing effort to develop high-speed switches for a variety of stationary and portable electronic equipment. As explained below, these devices offer advantages over electrostatically actuated micro-electromechanical switches, which, heretofore, have represented the state of the art of rapid, highly miniaturized electromechanical switches. Potential applications for these devices include computer memories, cellular telephones, communication networks, scientific instrumentation, and general radiation-hard electronic equipment.

A representative device of the present type includes a single-wall carbon nanotube suspended over a trench about 130 nm wide and 20 nm deep in an electrically insulating material. The ends of the carbon nanotube are connected to metal electrodes, denoted the source and drain electrodes. At bottom of the trench is another metal electrode, denoted the pull electrode (see figure). In the "off" or "open" switch state, no voltage is applied, and the nanotube remains out of contact with the pull elec-



A Carbon Nanotube Is Suspended between source and drain electrodes over a pull electrode. By application of a suitable potential (typically a few volts), the nanotube is drawn into contact with the pull electrode.

trode. When a sufficiently large electric potential (switching potential) is applied between the pull electrode and either or both of the source and drain electrodes, the resulting electrostatic attraction bends and stretches the nanotube into contact with the pull electrode, thereby putting the switch into the "on" or "closed" state, in which substantial current (typically as much as hundreds of nanoamperes) is conducted.

Devices of this type for use in initial experiments were fabricated on a thermally oxidized Si wafer, onto which Nb was

sputter-deposited for use as the pull-electrode layer. Nb was chosen because its refractory nature would enable it to withstand the chemical and thermal conditions to be subsequently imposed for growing carbon nanotubes. A 200-nm-thick layer of SiO₂ was formed on top of the Nb layer by plasma-enhanced chemical vapor deposition. In the device regions, the SiO₂ layer was patterned to thin it to the 20-nm trench depth. The trenches were then patterned by electron-beam lithography and formed by reactive-ion etching of the pattern through the 20-nm-thick SiO₂ to the Nb layer.

A 0.5-nm-thick layer of Fe was deposited, then patterned into catalyst islands for initiating growth of carbon nanotubes by means of photolithography and liftoff. To grow the carbon nanotubes, the workpiece as processed thus far was then placed in a chemical-vapor-deposition furnace, wherein it was exposed to an atmosphere of flowing CH₄ and H₂ at a temperature of 850 °C for 10 minutes. Next, a layer of Au/Ti was deposited and patterned in a lift-off process to form the source and drain electrodes in contact with the ends of the nanotubes.

Tests have confirmed the expected advantages of these devices over the older

electrostatically actuated microelectromechanical switches, which are characterized by response times of ≈1 μs and switching potentials between 60 and 70 V. The present devices are not only smaller but are characterized by response times of a few nanoseconds and switching potentials of a few volts. Hence, the present devices are expected to be better suited for applications in which there are requirements for highly miniaturized, high-speed electronic switches that can be operated from low-voltage (e.g., battery) power sources.

This work was done by Anupama Kaul, Eric Wong, and Larry Epp of Caltech for NASA's Jet Propulsion Laboratory.

In accordance with Public Law 96-517, the contractor has elected to retain title to this invention. Inquiries concerning rights for its commercial use should be addressed to:

*Innovative Technology Assets Management
JPL*

Mail Stop 202-233

4800 Oak Grove Drive

Pasadena, CA 91109-8099

(818) 354-2240

E-mail: iaoffice@jpl.nasa.gov

Refer to NPO-43343, volume and number of this NASA Tech Briefs issue, and the page number.

Solid-State High-Temperature Power Cells

These cells can be used in batteries for high-temperature applications.

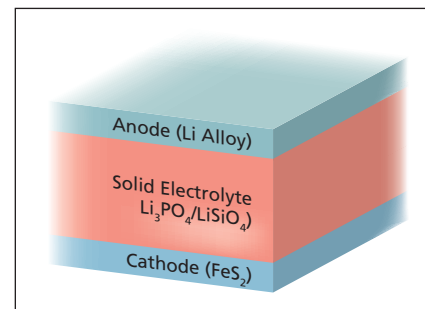
NASA's Jet Propulsion Laboratory, Pasadena, California

All-solid-state electrochemical power cells have been fabricated and tested in a continuing effort to develop batteries for instruments for use in environments as hot as 500 °C. Batteries of this type are needed for exploration of Venus, and could be used on Earth for such applications as measuring physical and chemical conditions in geothermal and oil wells, processing furnaces, and combustion engines.

In the state-of-the-art predecessors of the present solid-state power cells, fully packaged molten eutectic salts are used as electrolytes. The molten-salt-based cells can be susceptible to significant amounts of self-discharge and corrosion when used for extended times at elevated temperatures. In contrast, all-solid-state cells such as the present ones are expected to be capable of operating for many days at temperatures up to 500 °C, without significant self-discharge.

The solid-state cell described here includes a cathode made of FeS₂, an electrolyte consisting of a crystalline solid solution of equimolar amounts of Li₃PO₄ and Li₄SiO₄, and an anode made of an alloy of Li and Si (see figure). The starting material for making the solid electrolyte is a stoichiometric mixture of Li₃PO₄, SiO₂, and Li₃CO₂. This mixture is ball-milled, then calcined for two hours at a temperature of 1,100 °C, then placed in a die atop the cathode material. Next, the layers in the die are squeezed together at a pressure between 60 and 120 MPa for one hour at a temperature of 600 °C to form a unitary structure comprising the solid electrolyte and cathode bonded together. Finally, the lithium-alloy anode is pressure-bonded to the solid electrolyte layer, using an intermediate layer of pure lithium.

In one test of a cell of this type, a discharge rate of about 1 mA per gram of cathode material was sustained for 72



This **All-Solid-State Cell** is capable of generating electric power at a temperature up to 500 °C.

hours at a temperature of about 460 °C. This is about three times the discharge rate required to support some of the longer duration Venus-exploration mission scenarios.

This work was done by Jay Whitacre and William West of Caltech for NASA's Jet Propulsion Laboratory. Further information is contained in a TSP (see page 1). NPO-44396

Fast Offset Laser Phase-Locking System

Phases can be locked within a microcycle; known phase noise can be added.

NASA's Jet Propulsion Laboratory, Pasadena, California

Figure 1 shows a simplified block diagram of an improved optoelectronic system for locking the phase of one laser to that of another laser with an adjustable offset frequency specified by the user. In comparison with prior systems, this system exhibits higher performance (in-

cluding higher stability) and is much easier to use. The system is based on a field-programmable gate array (FPGA) and operates almost entirely digitally; hence, it is easily adaptable to many different systems. The system achieves phase stability of less than a microcycle.

It was developed to satisfy the phase-stability requirement for a planned spaceborne gravitational-wave-detecting heterodyne laser interferometer (LISA). The system has potential terrestrial utility in communications, lidar, and other applications.

The present system includes a fast phasemeter that is a companion to the microcycle-accurate one described in “High-Accuracy, High-Dynamic-Range Phase-Measurement System” (NPO-41927), *NASA Tech Briefs*, Vol. 31, No. 6 (June 2007), page 22. In the present system (as in the previously reported one), beams from the two lasers (here denoted the master and slave lasers) interfere on a photodiode. The heterodyne photodiode output is digitized and fed to the fast phasemeter, which produces suitably conditioned, low-latency analog control signals which lock the phase of the slave laser to that of the master laser. These control signals are used to drive a thermal and a piezoelectric transducer that adjust the frequency and phase of the slave-laser output.

The output of the photodiode is a heterodyne signal at the difference between the frequencies of the two lasers. (The difference is currently required to be less than 20 MHz due to the Nyquist limit of the current sampling rate. We foresee few problems in doubling this limit using current equipment.) Within the phasemeter, the photodiode-output signal is digitized to 15 bits at a sampling frequency of 40 MHz by use of the same analog-to-digital converter (ADC) as that of the previously reported phasemeter. The ADC output is passed to the FPGA, wherein the signal is demodulated using a digitally generated oscillator signal at the offset locking frequency specified by the user. The demodulated signal is low-pass filtered, decimated to a sample rate of 1 MHz, then filtered again. The decimated and filtered signal is converted to an analog output by a 1 MHz, 16-bit digital-to-analog converters. After a simple low-pass filter, these analog signals drive the thermal and piezoelectric transducers of the laser.

Although the system phase-locks the two lasers to within a microcycle, in the original application, there is an occasional need to analyze the performance of the phasemeter in the presence of noise in the difference between the

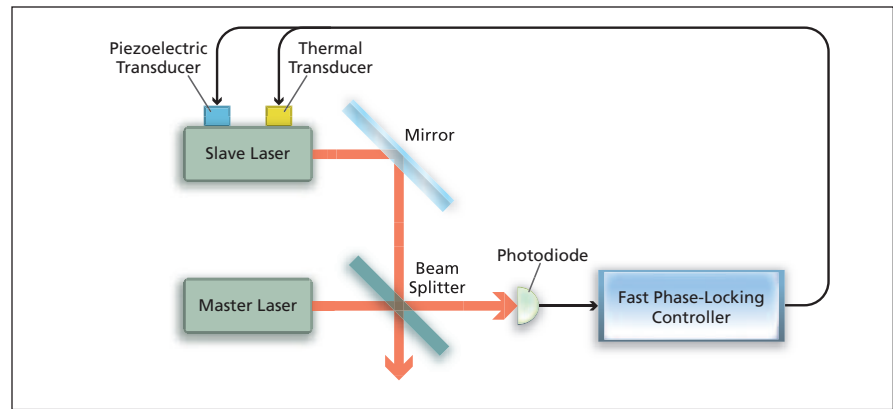


Figure 1. In the **Fast Offset Laser Phase-Locking System**, as in other such systems, a control signal is derived from the heterodyne signal arising from interference of two laser beams on a photodiode. The main innovative features of this system are embodied in the fast phase-locking controller, which is based on a mostly digital phasemeter.

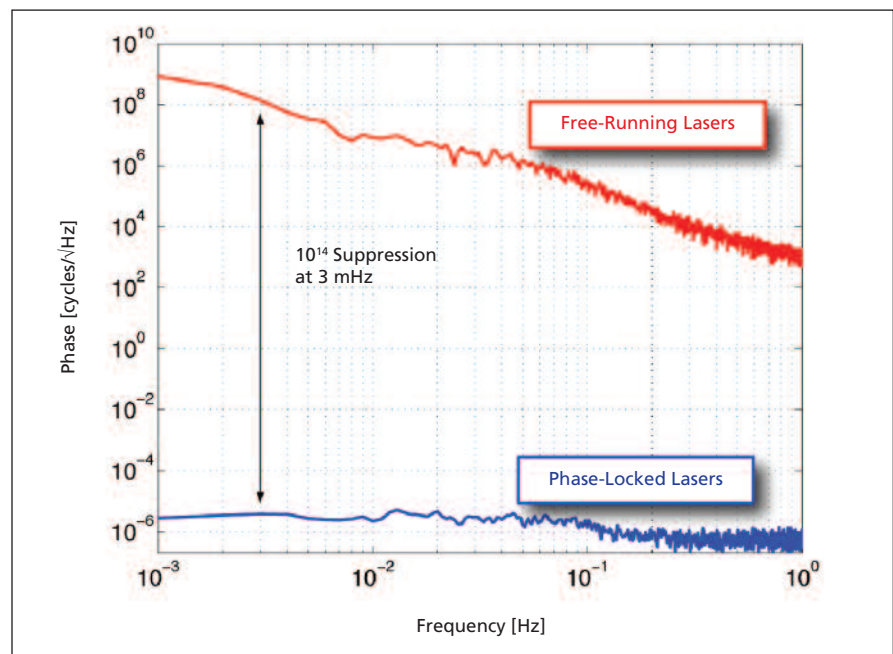


Figure 2. The **Performance of the Fast Offset Laser Phase-Locking System** is shown, as measured over the signal band, by the phasemeter described in NPO-41927.

phases and frequencies between the two lasers. This system includes a subsystem, based on a pseudorandom-number generator, that can add an adjustable amplitude phase noise characterized by a uniform, Gaussian, or $1/f$ distributions (where f denotes frequency). Figure 2 shows the per-

formance of the phase-locking system, and also noise added by the pseudorandom noise generator to mimic that of free-running lasers.

This work was done by Daniel Shaddock and Brent Ware of Caltech for NASA's Jet Propulsion Laboratory. Further information is contained in a TSP (see page 1). NPO-44740



Fabricating High-Resolution X-Ray Collimators

Goddard Space Flight Center, Greenbelt, Maryland

A process and method for fabricating multi-grid, high-resolution rotating modulation collimators for arcsecond and sub-arcsecond x-ray and gamma-ray imaging involves photochemical machining and precision stack lamination. The special fixturing and etching techniques that have been developed are used for the fabrication of multiple

high-resolution grids on a single array substrate.

This technology has application in solar and astrophysics and in a number of medical imaging applications including mammography, computed tomography (CT), single photon emission computed tomography (SPECT), and gamma cameras used in nuclear medi-

cine. This collimator improvement can also be used in non-destructive testing, hydrodynamic weapons testing, and microbeam radiation therapy.

This work was done by Michael Appleby, James E. Atkinson, Iain Fraser, and Jill Klinger of Mikro Systems, Inc. for Goddard Space Flight Center. Further information is contained in a TSP (see page 1). GSC-15275-1

Embossed Teflon AF Laminate Membrane Microfluidic Diaphragm Valves

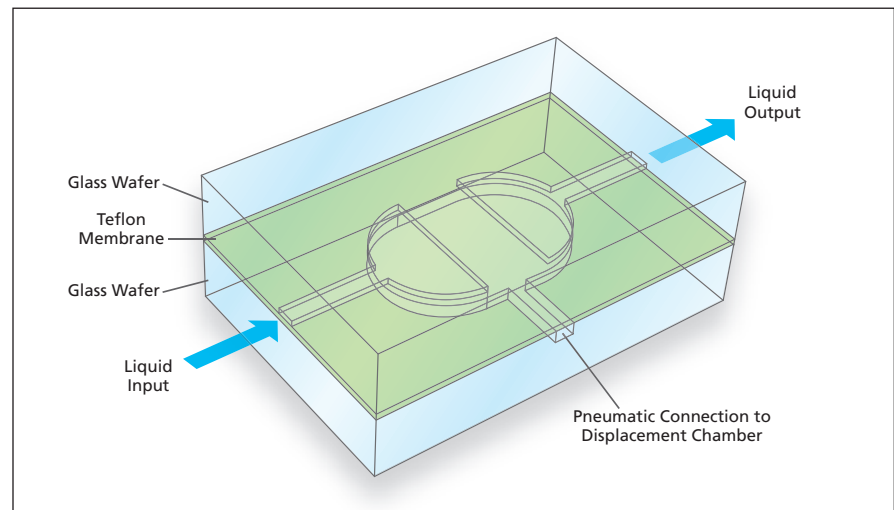
A new fabrication strategy for valve manifolds uses flexible, durable materials.

NASA's Jet Propulsion Laboratory, Pasadena, California

A microfluidic system has been designed to survive spaceflight and to function autonomously on the Martian surface. It manipulates microscopic quantities of liquid water and performs chemical analyses on these samples to assay for the presence of molecules associated with past or present living processes. This technology lies at the core of the Urey Instrument, which is scheduled for inclusion on the Pasteur Payload of the ESA ExoMars rover mission in 2013.

Fabrication processes have been developed to make the microfabricated Teflon-AF microfluidic diaphragm pumps capable of surviving extreme temperature excursions before and after exposure to liquid water. Two glass wafers are etched with features and a continuous Teflon membrane is sandwiched between them (see figure). Single valves are constructed using this geometry.

The microfabricated devices are then post processed by heating the assembled device while applying pneumatic pressure to force the Teflon diaphragm against the valve seat while it is softened. After cooling the device, the "embossed" membrane retains this new shape. This solves previous problems with bubble introduction into the fluid flow where deformations of the membrane at the valve seat occurred during device bonding at el-



The Valve Assembly consists of two glass wafers with a continuous Teflon membrane sandwiched between them.

evated temperatures (100–150 °C). The use of laminated membranes containing commercial Teflon AF 2400 sheet sandwiched between spun Teflon AF 1600 layers performed best, and were less gas permeable than Teflon AF 1600 membranes on their own.

Spinning Teflon AF 1600 solution (6 percent in FLOURINERT® FC40 solvent, 3M Company) at 500 rpm for 1.5 seconds, followed by 1,000 rpm for 3 seconds onto Borofloat glass wafers, results in a 10-micron-thick film of ex-

tremely smooth Teflon AF. This spinning process is repeated several times on flat, blank, glass wafers in order to gradually build a thick, smooth membrane. After running this process at least five times, the wafer and Teflon coating are heated under vacuum at 220 °C for one hour in order to drive off any residual solvent present in the composite film. After this, a second blank, glass wafer is brought down from above and the stack is held under vacuum at 3 atm mechanical pressure for ten 10 hours.

These membranes are released from the bonding stack by placing the whole stack in 49-percent HF solution, which dissolves the glass wafers completely. After thorough rinsing and drying, the membrane is ready for bonding in a device by holding it under 3 atm pressure and temperatures of at least 120 °C for 10 hours.

Microfabricated devices are mounted onto an aluminum baseplate that rests on a hot plate. The entire assembly is positioned underneath a binocular optical microscope for real-time visual inspection. Pneumatic connections are made to the valve input, output, and

displacement chamber via Tygon tubing. Air pressure of 10 psi (69 kPa) is applied to the underside of the membrane, and the device is slowly heated. A slight pressure [0.5 psi (35 kPa)] is applied to the input gas connection, and the output is directed into a beaker of water. When the temperature rises to approximately 160 °C in the membrane area, the flow rate through the valve (i.e., bubbles forming in beaker per unit time) drops sharply and shifting patterns of Newton rings can be observed in the valve seat. After cooling the device to room temperature, the single valve sealing characteristics are

drastically improved. The liquid flow rate through the device is measured as a function of pressure in the displacement chamber for a given applied input pressure of 0.5 psi (35 kPa). Flow rates are determined by measuring time required to fill a known tube volume. Embedding a higher melting temperature Teflon AF polymer core in the center of the membrane improved valve performance further.

This work was done by Peter Willis, Brian Hunt, Victor White, and Frank Grunthaner of Caltech for NASA's Jet Propulsion Laboratory. For more information, contact iaoffice@jpl.nasa.gov. NPO-44975



⚙️ Flipperons for Improved Aerodynamic Performance

For a given airfoil design, lift is increased and drag reduced.

Langley Research Center, Hampton, Virginia

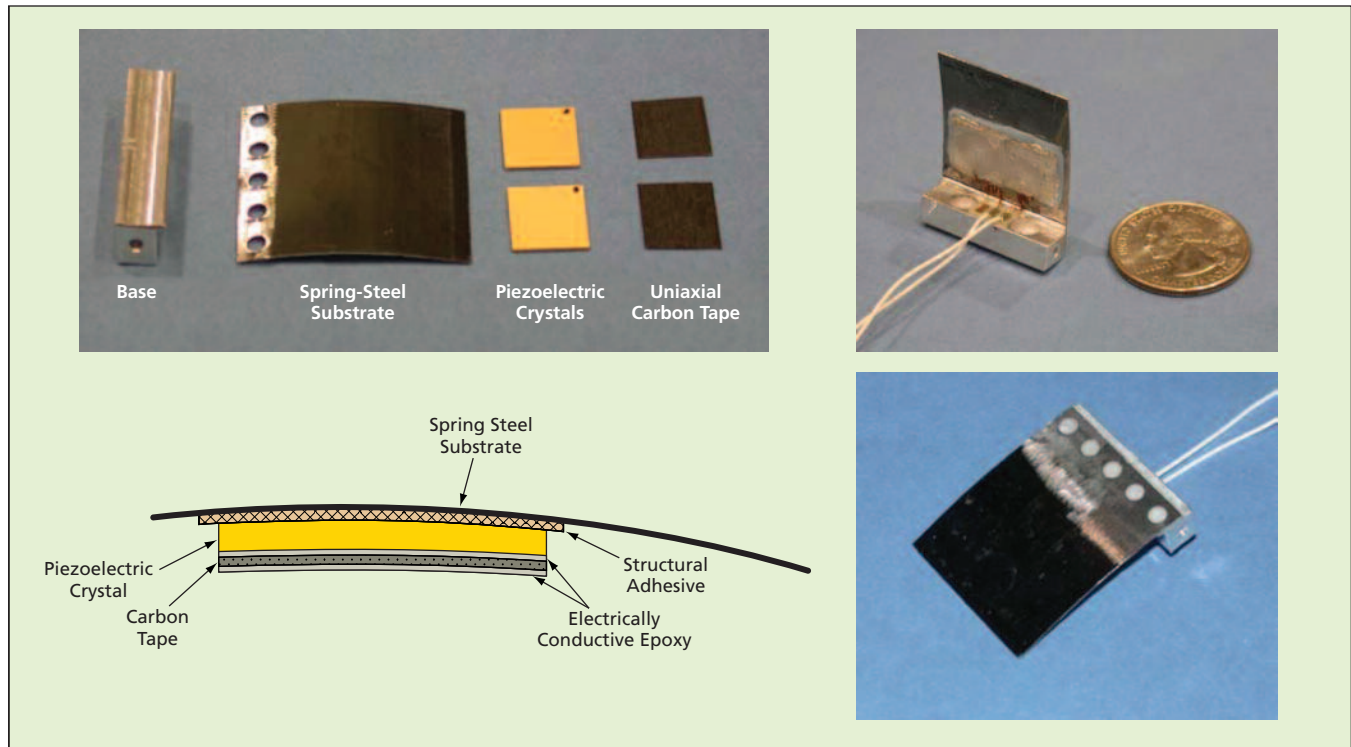


Figure 1. The Piezoelectric Crystal in a lightweight bending actuator is maintained in compressive preload by a spring-steel substrate.

Lightweight, piezoelectrically actuated bending flight-control surfaces have shown promise as means of actively controlling airflows to improve the performances of transport airplanes. These bending flight-control surfaces are called “flipperons” because they look somewhat like small ailerons, but, unlike ailerons, are operated in an oscillatory mode reminiscent of the actions of biological flippers.

The underlying concept of using flipperons and other flipperlike actuators to impart desired characteristics to flows is not new. Moreover, elements of flipperon-based active flow-control (AFC) systems for aircraft had been developed previously, but it was not until the development reported here that the elements have been integrated into a complete, controllable prototype AFC system for wind-tunnel testing to enable evaluation of the benefits of AFC for aircraft.

The piezoelectric actuator materials chosen for use in the flipperons are single-crystal solid solutions of lead zinc

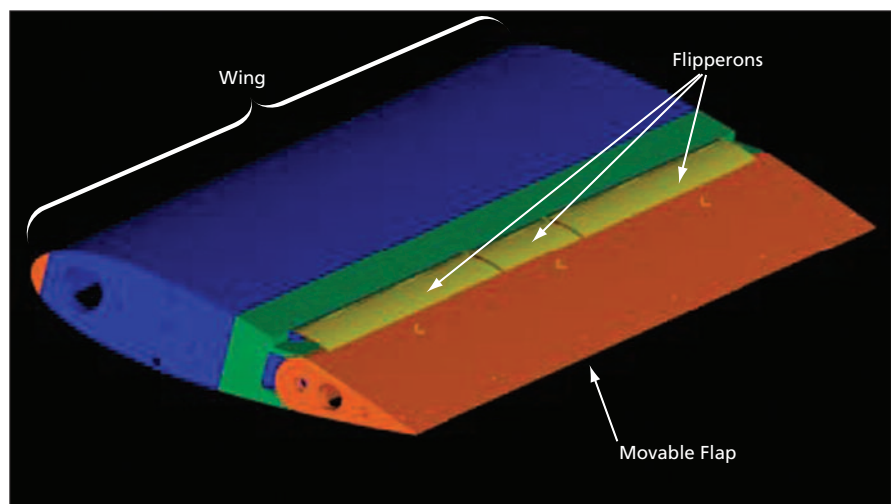


Figure 2. Flipperons on the Upper Surface of a wing are made to oscillate at amplitude, frequency, and phase chosen to obtain increased lift and reduced drag.

niobate and lead titanate, denoted generically by the empirical formula $(1-x)[\text{Pb}(\text{Zn}_{1/3}\text{Nb}_{2/3})\text{O}_3]:x[\text{PbTiO}_3]$ (where $x < 1$) and popularly denoted by the abbreviation “PZN-PT.” These are

relatively newly recognized piezoelectric materials that are capable of strain levels exceeding 1 percent and strain-energy densities 5 times greater than those of previously commercially available piezo-

electric materials. Despite their high performance levels, $(1-x)[\text{Pb}(\text{Zn}_{1/3}\text{Nb}_{2/3})\text{O}_3]:x[\text{PbTiO}_3]$ materials have found limited use until now because, relative to previously commercially available piezoelectric materials, they tend to be much more fragile.

What has made it feasible to incorporate $(1-x)[\text{Pb}(\text{Zn}_{1/3}\text{Nb}_{2/3})\text{O}_3]:x[\text{PbTiO}_3]$ crystals into flipperons is a design and fabrication approach in which the crystals are preloaded and reinforced so as to minimize exposure to tensile stresses, which could break them. The essence of this approach is to place the piezoelectric crystals in each actuator under a compressive preload along the fore-and-aft axis and to bond tapes of uniaxial carbon fibers to the outer surfaces of the crystals to minimize lateral tensile strain in each crystal (see Figure 1). By minimizing tensile strains in the crystals, one minimizes crystal damage, thereby minimizing the probability of actuator failure.

The prototype AFC system includes not only flipperons but also flipperon-displacement position sensors, a power subsystem, and a control subsystem. For initial tests, the flipperons were installed on the upper surface of a standard airfoil (wing) model at the flap hinge (see Figure 2). The model was mounted in a low-speed wind tunnel at the University of Arizona, where the tests were performed. The tests included measurements of customary aerodynamic-performance parameters (e.g., coefficients of lift and drag) at various angles of attack and airspeeds. During these tests, the flipperons were actuated at various amplitudes, frequencies, and phases.

The tests showed that with appropriate actuation of flipperons, lift was increased and drag reduced, by amounts of the order of a percent. Data from these tests were then used to estimate the benefits that could be obtained by adding flipperon-based AFC systems to

transport airplanes in two tests cases. In one case, it was found that the addition of the flipperons to the vertical stabilizer of a Boeing 777 (or equivalent) airplane would make it possible to reduce the size of the vertical stabilizer, thereby reducing the drag, by an amount sufficient to enable a reduction of fuel consumption by as much as 1.7 percent. In another case, it was found that by exploiting the ability of a flipperon-based AFC system to delay the onset of stall, one could safely increase the angle of attack (thereby increasing lift) while reducing the size of the wings (thereby reducing the weight) of a blended-wing/body airplane by an amount sufficient to enable a reduction of fuel consumption by as much as 0.6 percent.

*This work was done by James H. Mabe of The Boeing Co. for Langley Research Center. Further information is contained in a TSP (see page 1).
LAR-17172-1*

System Estimates Radius of Curvature of a Segmented Mirror

Marshall Space Flight Center, Alabama

A system that estimates the global radius of curvature (GRoC) of a segmented telescope mirror has been developed for use as one of the subsystems of a larger system that exerts precise control over the displacements of the mirror segments. This GRoC-estimating system, when integrated into the overall control system along with a mirror-segment-actuation subsystem and edge sensors (sensors that measure displacements at selected points on the edges of the segments), makes it possible to control the GRoC mirror-deformation mode, to which mode contemporary edge sensors are insufficiently sensitive.

This system thus makes it possible to control the GRoC of the mirror with sufficient precision to obtain the best possible image quality and/or to impose a required wavefront correction on incoming or outgoing light.

In its mathematical aspect, the system utilizes all the information available from the edge-sensor subsystem in a unique manner that yields estimates of all the states of the segmented mirror. The system does this by exploiting a special set of mirror boundary conditions and mirror influence functions in such a way as to sense displacements in degrees of freedom that would other-

wise be unobservable by means of an edge-sensor subsystem, all without need to augment the edge-sensor system with additional metrological hardware. Moreover, the accuracy of the estimates increases with the number of mirror segments.

This work was done by John Rakoczy of Marshall Space Flight Center.

This invention has been patented by NASA (U.S. Patent No. 7,050,161). Inquiries concerning nonexclusive or exclusive license for its commercial development should be addressed to Sammy Nabors, MSFC Commercialization Assistance Lead, at sammy.a.nabors@nasa.gov. Refer to MFS-31807-1.



Refractory Ceramic Foams for Novel Applications

Properties could be tailored for specific uses as insulators, filters, or catalyst supports.

Ames Research Center, Moffett Field, California

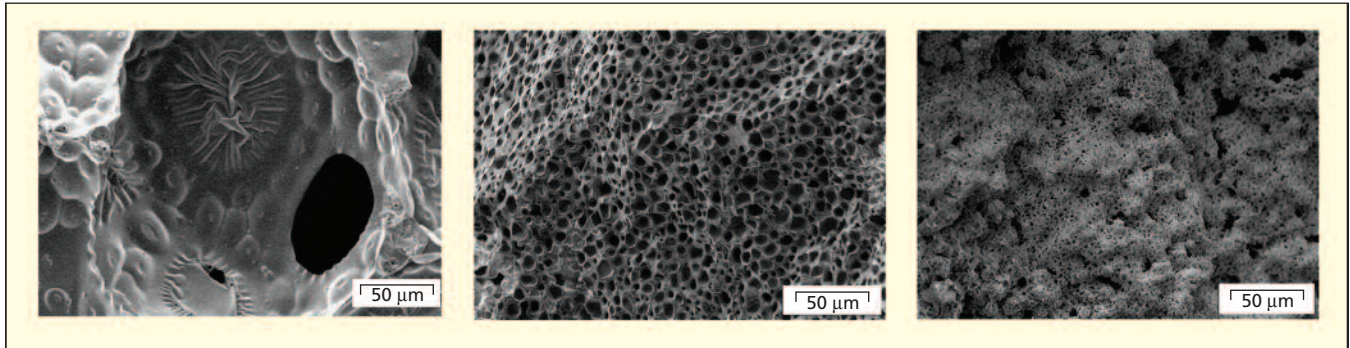


Figure 1. These Microstructures Are Typical of ceramic foams made by pyrolysis of preceramic polymers with sacrificial blowing agents and/or sacrificial fillers.

Workers at NASA Ames Research center are endeavoring to develop durable, oxidation-resistant, foam thermal protection systems (TPSs) that would be suitable for covering large exterior spacecraft surfaces, would have low to moderate densities, and would have temperature capabilities comparable to those of carbon-based TPSs [reusable at 3,000 °F ($\approx 1,650$ °C)] with application of suitable coatings. These foams may also be useful for repairing TPSs while in orbit. Moreover, on Earth as well as in outer space, these foams might be useful as catalyst supports and filters.

Preceramic polymers are obvious candidates for use in making the foams in question. The use of these polymers offers advantages over processing routes followed in making conventional ceramics. Among the advantages are the ability to plastically form parts, the ability to form pyrolyzed ceramic materials at lower temperatures, and the ability to form high-purity microstructures having properties that can be tailored to satisfy requirements.

Heretofore, preceramic polymers have been used mostly in the production of such low-dimensional products as fibers because the loss of volatiles during pyrolysis of the polymers leads to porosity and large shrinkage (in excess of 30 percent). In addition, efforts to form bulk structures from preceramic polymers have resulted in severe cracking during pyrolysis. However, because the foams in question would consist of networks of thin struts (in contradistinction

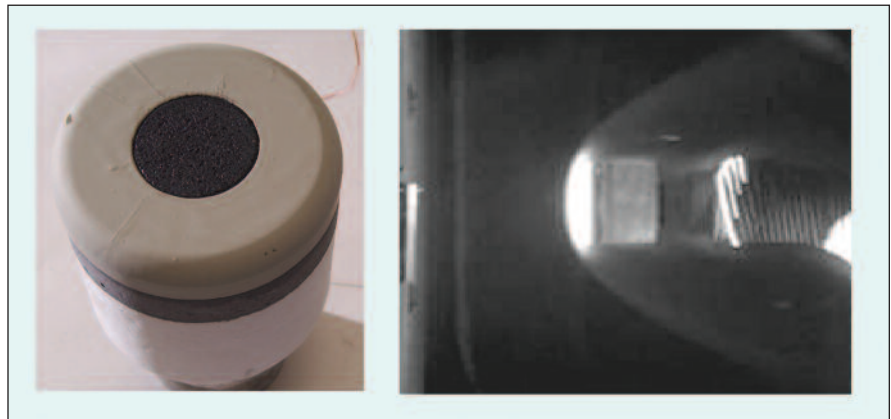


Figure 2. An Arc Jet Test Model is shown before and during testing. The material specimen to be tested is the black disk in the center.

to nonporous dense solids), these foams are ideal candidates for processing along a preceramic-polymer route.

The present research explores the feasibility of forming ceramic foams using sacrificial blowing agents and/or sacrificial fillers in combination with preceramic polymers. The possibility of using reactive fillers in combination with the aforementioned ingredients is also investigated. The use of such reactive fillers as Ti or Si reduces the large shrinkage observed in pyrolysis of polymers. The fillers also react with excess carbon that, in the absence of such reaction, would be present in the foam pyrolysis products. A reactive filler becomes converted to a ceramic material with an expansion that reduces overall shrinkage in the pyrolyzed part. The expansion of the reac-

tive filler thus compensates for the shrinkage of the polymer if the appropriate volume fraction of filler is present in a reactive atmosphere (e.g., N_2 or NH_3).

Previously, this reactive-filler approach yielded limited success in efforts to make fully dense structural composite materials (in contradistinction to foams). However, in the present research, this reactive-filler approach has been modified to enable processing of foams with minimal shrinkage.

Figure 1 shows representative foam microstructures. In all cases, the foams are isotropic, open-celled structures. Foams processed by use of a polyurethane blowing agent have large cell sizes (50 to 500 μm), whereas foams processed by incorporating sacrificial fillers (e.g., polymer microspheres) generally have much

smaller cell sizes (as low as 3 μm , depending on the diameter of the starting sacrificial filler particles). In all three micrographs of Figure 1, it is evident that the original unpyrolyzed structure is retained after pyrolysis, without loss of spherical cell shape.

In preliminary tests, specimens of SiC foams made by processing from pre-ceramic polymers were exposed to arc jets, which are traditionally used to simulate the aerothermal heating environments experienced by spacecraft entering or re-entering a planetary atmosphere. These tests were con-

ducted in the NASA Ames 60-MW Interaction Heating Facility (IHF), wherein flowing air is heated by an electric discharge. In these tests, disk specimens of 1.5-in. (3.81-cm) diameter and 0.5-in. (1.27-cm) thickness were mounted in an SiC-coated graphite holder and exposed to a temperature of 1,650 $^{\circ}\text{C}$ for 90 seconds (see Figure 2). The specimens showed minimal degradation after exposure.

In summary, the use of pre-ceramic polymers with the addition of sacrificial blowing agents and sacrificial and/or reactive fillers offers a feasible approach to

forming open-cell ceramic foams. Moreover, it has been found that refractory ceramic foams having properties that are encouraging for further development can be made using processing temperatures that, for ceramics, are relatively low ($\approx 1,200$ $^{\circ}\text{C}$). This approach enables tailoring of such foam properties as composition, pore size, and strength by varying the processing conditions.

This work was done by M. Stackpoole of ELORET for Ames Research Center. Further information is contained in a TSP (see page 1). ARC-15260-1

Self-Deploying Trusses Containing Shape-Memory Polymers

Compacted structures can be used in shelters for hostile environments.

John H. Glenn Research Center, Cleveland, Ohio

Composite truss structures are being developed that can be compacted for stowage and later deploy themselves to full size and shape. In the target applications, these “smart” structures will precisely self-deploy and support a large, lightweight space-based antenna. Self-deploying trusses offer a simple, light, and affordable alternative to articulated mechanisms or inflatable structures. The trusses may also be useful in such terrestrial applications as variable-geometry aircraft components or shelters that can be compacted, transported, and deployed quickly in hostile environments.

The truss technology uses high-performance shape-memory-polymer (SMP) thermoset resin reinforced with fibers to form a helical composite structure. At normal operating temperatures, the truss material has the structural properties of a conventional composite. This enables truss designs with required torsion, bending, and compression stiffness. However, when heated to its designed glass transition temperature (T_g), the SMP matrix acquires the flexibility of an elastomer. In this state, the truss can be compressed telescopically to a configuration encompassing a fraction of its original volume.

When cooled below T_g , the SMP reverts to a rigid state and holds the truss in the stowed configuration without external constraint. Heating the materials above T_g activates truss deployment as the composite material releases strain energy, driving the truss to its original “memorized” configuration without the



Activation Sequence of an early prototype self-deploying truss shows one one-minute duration from compressed [2.5 in. (6.4 cm)] to deployed [28.5 in. (72.4 cm)].

need for further actuation. Laboratory prototype trusses have demonstrated repeatable self-deployment cycles following linear compaction exceeding an 11:1 ratio (see figure).

While this new truss technology exhibits some functionality similar to that of cold hibernated elastic memory (CHEM) structures developed in other NASA-sponsored research (previously reported in *NASA Tech Briefs*), there are important distinctions. First, the CHEM SMP is based on a thermoplastic resin, while the new truss material's high-performance SMP is a fully cured thermoset resin. The high-perform-

ance SMP molecular design has been implemented in a variety of resin systems, enabling resin selection for desired structural properties while enabling selection of a required T_g (e.g., 25–225 $^{\circ}\text{C}$ achievable in high-performance SMPs based on cyanate ester). Also, CHEM-based structures use unreinforced foam as the active component. In the new composite truss design, the high-performance SMP is integral to the structure, simplifying the design and increasing the savings in mass, cost, and system complexity. Structures employing high-performance SMP are fabricated using the

same processes as conventional composites. The composite structure's mechanical properties at temperatures below T_g are unaffected by repeated stowage-deployment cycles.

This work was done by Robert M. Schueler of Cornerstone Research Group, Inc. for Glenn Research Center.

Inquiries concerning rights for the commercial use of this invention should be addressed

to NASA Glenn Research Center, Innovative Partnerships Office, Attn: Steve Fedor, Mail Stop 4-8, 21000 Brookpark Road, Cleveland, Ohio 44135. Refer to LEW-17982-1.

Fuel-Cell Electrolytes Based on Organosilica Hybrid Proton Conductors

NASA's Jet Propulsion Laboratory, Pasadena, California

A new membrane composite material that combines an organosilica proton conductor with perfluorinated Nafion material to achieve good proton conductivity and high-temperature performance for membranes used for fuel cells in stationary, transportation, and portable applications has been developed.

To achieve high proton conductivities of the order of $10^{-1} \text{S}\cdot\text{cm}^{-1}$ over a wide range of temperatures, a composite membrane based on a new class of mesoporous, proton-conducting, hydrogen-

bonded organosilica, used with Nafion, will allow for water retention and high proton conductivity over a wider range of temperatures than currently offered by Nafion alone. At the time of this reporting, this innovation is at the concept level. Some of the materials and processes investigated have shown good proton conductivity, but membranes have not yet been prepared and demonstrated.

This work was done by Sri R. Narayan and Shiao-Pin S. Yen of Caltech for NASA's Jet Propulsion Laboratory.

In accordance with Public Law 96-517, the contractor has elected to retain title to this invention. Inquiries concerning rights for its commercial use should be addressed to:

Innovative Technology Assets Management: JPL, Mail Stop 202-233, 4800 Oak Grove Drive, Pasadena, CA 91109-8099, (818) 354-2240, E-mail: iaoffice@jpl.nasa.gov.

Refer to NPO-40228, volume and number of this NASA Tech Briefs issue, and the page number.

Molecules for Fluorescence Detection of Specific Chemicals

These molecules could be used in the detection of chemical warfare agents.

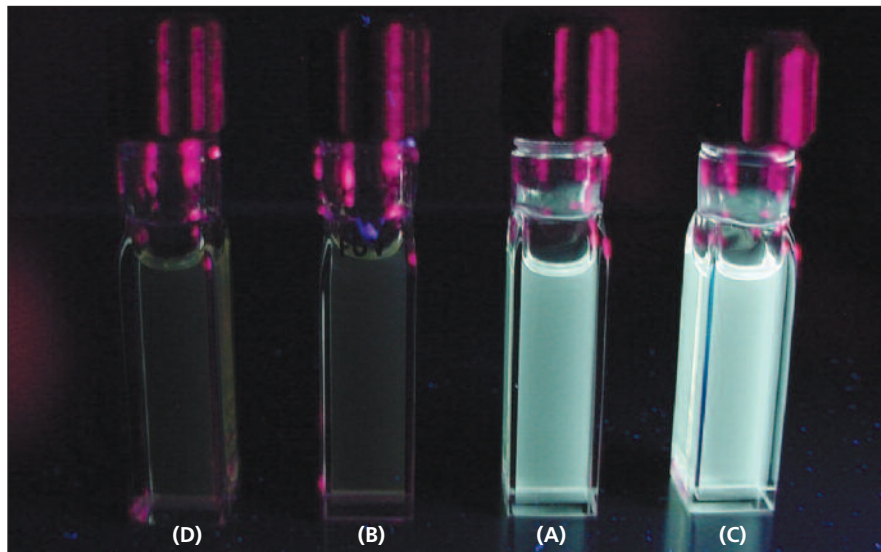
John H. Glenn Research Center, Cleveland, Ohio

A family of fluorescent dye molecules has been developed for use in "on-off" fluorescence detection of specific chemicals. By themselves, these molecules do not fluoresce. However, when exposed to certain chemical analytes in liquid or vapor forms, they do fluoresce (see figure). These compounds are amenable to fixation on or in a variety of substrates for use in fluorescence-based detection devices: they can be chemically modified to anchor them to porous or non-porous solid supports or can be incorporated into polymer films. Potential applications for these compounds include detection of chemical warfare agents, sensing of acidity or alkalinity, and fluorescent tagging of proteins in pharmaceutical research and development. These molecules could also be exploited for use as two-photon materials for photodynamic therapy in the treatment of certain cancers and other diseases.

A molecule in this family consists of a fluorescent core (such as an anthracene or pyrene) attached to two

end groups that, when the dye is excited by absorption of light, transfer an electron to the core, thereby quenching the fluorescence. The end groups

can be engineered so that they react chemically with certain analytes. Upon reaction, electrons on the end groups are no longer available for transfer to



The Effects of Adding Different Analytes are illustrated on the activation of a fluorescent "on-off" sensor. Shown are sensor molecules before activation (D), after activation by treatment with acid (A), acid treated sample that has been deactivated by treatment with base (B), and sensor molecule activated by treatment with acetyl chloride (C).

the core and, consequently, the fluorescence from the core is no longer quenched.

The chemoselectivity of these molecules can be changed by changing the end groups. For example, aniline end groups afford a capability for sensing acids or acid halides (including those contained in chemical warfare agents). Pyridine or bipyridyl end groups would enable sensing of metal ions. Other

chemicals that can be selectively detected through suitable choice of end groups include glucose and proteins. Moreover, the fluorescent cores can be changed to alter light-absorption and -emission characteristics: anthracene cores fluoresce at wavelengths around 500 nm, whereas perylene cores absorb and emit at wavelengths of about 600 nm.

This work was done by Michael A. Meador of Glenn Research Center and Daniel S.

Tyson and Ulvi F. Ilhan of Ohio Aerospace Institute. Further information is contained in a TSP (see page 1).

Inquiries concerning rights for the commercial use of this invention should be addressed to NASA Glenn Research Center, Innovative Partnerships Office, Attn: Steve Fedor, Mail Stop 4-8, 21000 Brookpark Road, Cleveland, Ohio 44135. Refer to LEW-18059-1.



Cell-Detection Technique for Automated Patch Clamping

Candidate cells are identified automatically within one second.

John H. Glenn Research Center, Cleveland, Ohio

A unique and customizable machine-vision and image-data-processing technique has been developed for use in automated identification of cells that are

optimal for patch clamping. [Patch clamping (in which patch electrodes are pressed against cell membranes) is an electrophysiological technique widely

applied for the study of ion channels, and of membrane proteins that regulate the flow of ions across the membranes. Patch clamping is used in many biological

research fields such as neurobiology, pharmacology, and molecular biology.] While there exist several hardware techniques for automated patch clamping of cells, very few of those techniques incorporate machine vision for locating cells that are ideal subjects for patch clamping. In contrast, the present technique is embodied in a machine-vision algorithm that, in practical application, enables the user to identify “good” and “bad” cells for patch clamping in an image captured by a charge-coupled-device (CCD) camera attached to a microscope, within a processing time of one second. Hence, the present technique can save time, thereby increasing efficiency and reducing cost.

The present technique involves the utilization of cell-feature metrics to accurately make decisions on the degree to which individual cells are “good” or “bad” candidates for patch clamping. These metrics include position coordinates (x,y) in the image plane, major-axis length, minor-axis length, area, elongation, roundness, smoothness, angle of orientation, and degree of inclusion in the field of view.

The present technique does not require any special hardware beyond commercially available, off-the-shelf patch-clamping hardware: A standard patch-clamping microscope system with an attached CCD camera, a personal computer with an image-data-processing board, and some experience in utilizing image-data-processing software are all that are needed. A cell image is first captured by the microscope CCD camera and image-data-pro-

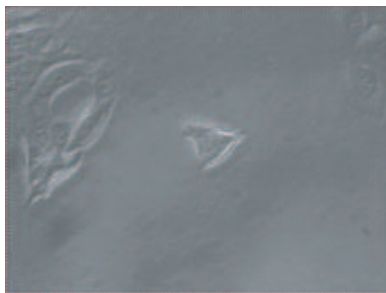
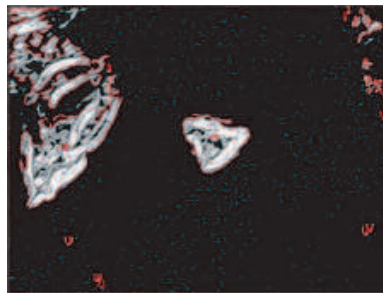
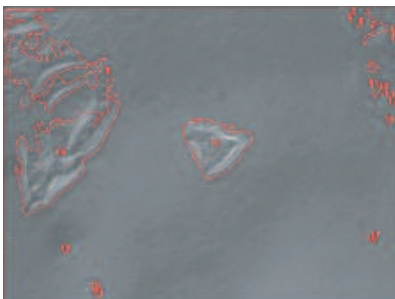


Image of Cells



Result of Applying "Find Particles" Technique to Image



Overlay of Identified Objects on Image of Cells



"Good" Candidate Cell for Patch Clamping

Number of Identified Object	x	y	Major-Axis Length	Minor-Axis Length	Area	Elongation	Roundness	Smoothness	Angle of Orientation	Thinness in Center	Partial Inclusion
1	72	89	191.8	126.7	12491	0.661	0.077	0.143	137	F	T
2	597	33	49.9	44.9	844	0.899	0.18	0.162	1.2	T	T
3	565	12	6.8	3.7	27	0.537	0.908	0.203	40.3	F	F
4	575	28	17.3	9.3	114	0.536	0.449	0.1	83.3	F	F
5	559	21	4	2.5	15	0.615	0.943	0.159	80.8	F	F
6	629	41	3.4	2.3	13	0.676	0.99	0.205	103.3	F	T
7	629	51	12	4	38	0.333	0.489	0.144	90	T	T
8	595	98	16	14	175	0.876	0.884	0.168	4.7	F	F
9	169	108	4	4	19	1	1.775	0.167	0	F	F
10	93	239	247.1	117.3	14243	0.475	0.093	0.139	44.7	T	F
11	599	129	35.8	14.6	277	0.409	0.323	0.185	99.4	F	F
12	614	132	22.1	5.5	121	0.25	0.361	0.161	76.5	F	F
13	623	146	5.4	1.9	15	0.346	0.619	0.135	74	F	F
14	630	158	3.2	1	7	0.302	0.752	0.188	74.5	F	T
15	342	223	122	88.4	6417	0.73	0.3	0.14	161	F	F
16	624	185	6.7	4.1	26	0.618	0.965	0.2	58.3	F	F
17	601	371	5.1	3.8	21	0.744	1.805	0.188	125.8	F	F
18	594	377	6.7	5	31	0.739	1.269	0.203	137.4	F	F
19	101	392	8	4.6	34	0.572	0.994	0.147	36	F	F
20	150	453	9.4	5	50	0.535	0.845	0.125	26.6	F	F
21	155	465	5.4	2.2	15	0.396	0.75	0.25	5.7	F	F

Note: Object 15 is the “best” candidate for patch clamping.

In this Example of Application of the technique described in the text, processing of an image of cells leads to identification of the approximately triangular object at the center as a “good” candidate cell for patch clamping. The table presents numerical results of analysis of 21 objects identified in the “find particles” stage of image-data processing.

cessing board, then the image data are analyzed by software that implements the present machine-vision technique. This analysis results in the identification of cells that are “good” candidates for patch clamping (see figure). Once a “good” cell is identified, a patch clamp can be effected by an automated patch-clamping apparatus or by a human operator.

This technique has been shown to enable reliable identification of “good”

and “bad” candidate cells for patch clamping. The ultimate goal in further development of this technique is to combine artificial-intelligence processing with instrumentation and controls in order to produce a complete “turnkey” automated patch-clamping system capable of accurately and reliably patch clamping cells with a minimum intervention by a human operator. Moreover, this technique can be adapted to virtually any cellular-analysis procedure that

includes repetitive operation of microscope hardware by a human.

This work was done by Mark McDowell of Glenn Research Center and Elizabeth Gray of Scientific Consulting, Inc. Further information is contained in a TSP (see page 1).

Inquiries concerning rights for the commercial use of this invention should be addressed to NASA Glenn Research Center, Innovative Partnerships Office, Attn: Steve Fedor, Mail Stop 4-8, 21000 Brookpark Road, Cleveland, Ohio 44135. Refer to LEW-17902-1.

Redesigned Human Metabolic Simulator

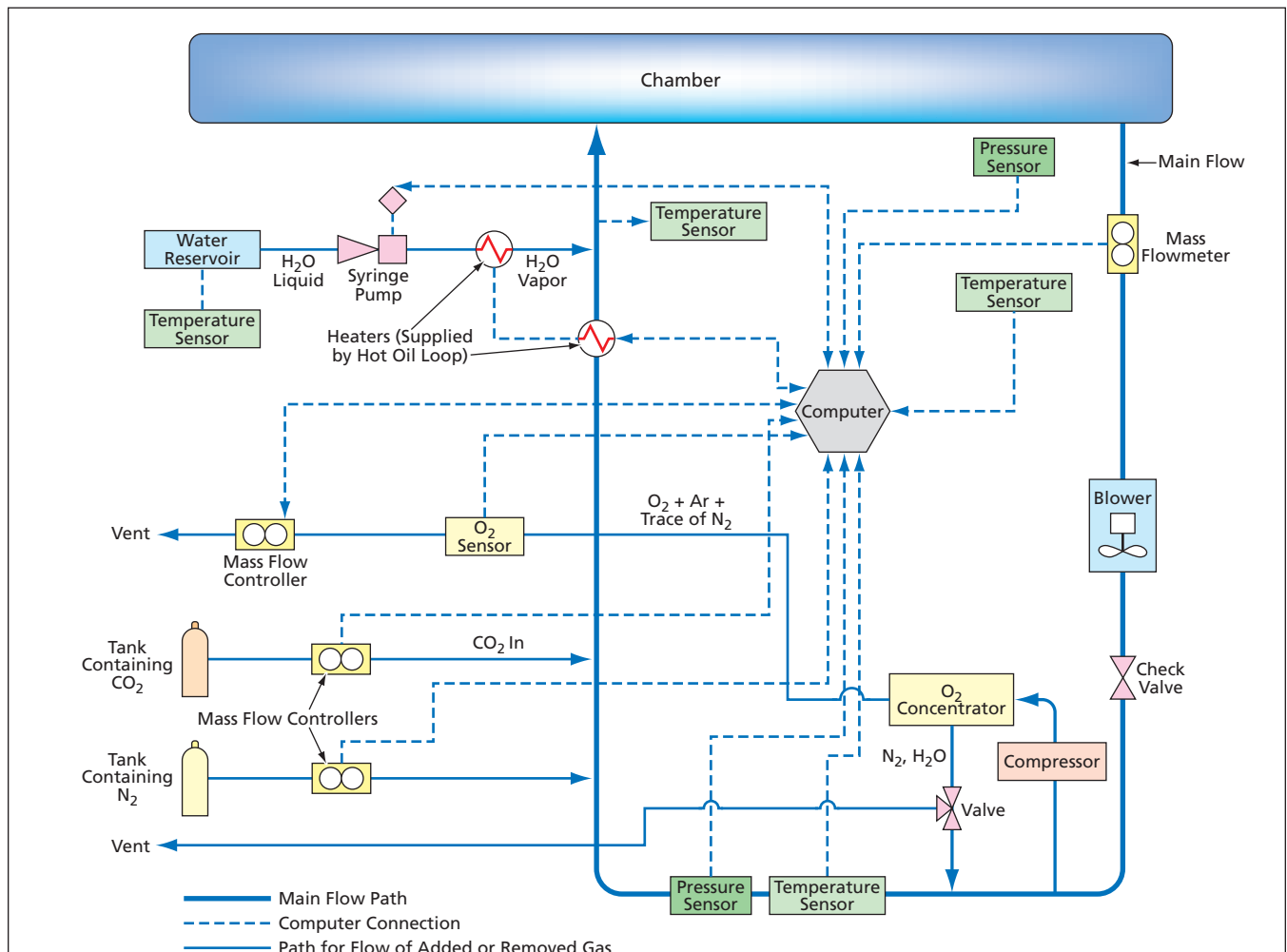
Apparatus simulates atmospheric effects of human respiration.

Lyndon B. Johnson Space Center, Houston, Texas

A design has been formulated for a proposed improved version of an apparatus that simulates atmospheric effects of human respiration by introducing controlled amounts of carbon dioxide,

water vapor, and heat into the air. Denoted a human metabolic simulator (HMS), the apparatus is used for testing life-support equipment when human test subjects are not available.

The prior version of the HMS, to be replaced, was designed to simulate the respiratory effects of as many as four persons. It exploits the catalytic combustion of methyl acetate, for which the respira-



The Improved HMS would remove O₂ while adding CO₂, H₂O, and heat in amounts chosen to simulate the respiratory effects of as many as eight humans at various levels of activity.

tory quotient (the molar ratio of carbon dioxide produced to oxygen consumed) is very close to the human respiratory quotient of about 0.86. The design of the improved HMS provides for simulation of the respiratory effects of as many as eight persons at various levels of activity. The design would also increase safety by eliminating the use of combustion.

The improved HMS (see figure) would include a computer that would exert overall control. The computer would calculate the required amounts of oxygen removal, carbon dioxide addition, water addition, and heat addition by use of empirical equations for metabolic profiles of respiration and heat.

A blower would circulate air between the HMS and a chamber containing a life-support system to be tested. With the help of feedback from a mass flowmeter, the blower speed would be adjusted to regulate the rate of flow ac-

ording to the number of persons to be simulated and to a temperature-regulation requirement (the air temperature would indirectly depend on the rate of flow, among other parameters).

Oxygen would be removed from the circulating air by means of a commercially available molecular sieve configured as an oxygen concentrator. Oxygen, argon, and trace amounts of nitrogen would pass through a bed in the molecular sieve while carbon dioxide, the majority of nitrogen, and other trace gases would be trapped by the bed and subsequently returned to the chamber. If, as recommended, the oxygen concentrator were of a rotating twelve-bed design, then variations in the product stream could be made very small.

Carbon dioxide would be added directly to the circulating air by simple injection from a supply tank. The rate of injection would be maintained at the required rate by use of a mass flowme-

ter/controller. In the same way, nitrogen would be added to make up for the small amount of nitrogen lost through the oxygen concentrator.

Water vapor would be added to the circulating air by heating the corresponding required flow of water to steam in a heat exchanger. More heat, required to complete the simulation of the thermal effect of respiration, would be added through another heat exchanger. Heat would be supplied to both heat exchangers via a hot-oil loop.

This work was done by Bruce Duffield, Frank Jeng, and Kevin Lange of Lockheed Martin Corp. for Johnson Space Center.

This invention is owned by NASA, and a patent application has been filed. Inquiries concerning nonexclusive or exclusive license for its commercial development should be addressed to the Patent Counsel, Johnson Space Center, (281) 483-0837. Refer to MSC-23846.



Compact, Highly Stable Ion Atomic Clock

This high-precision clock is designed for navigation and radio science applications.

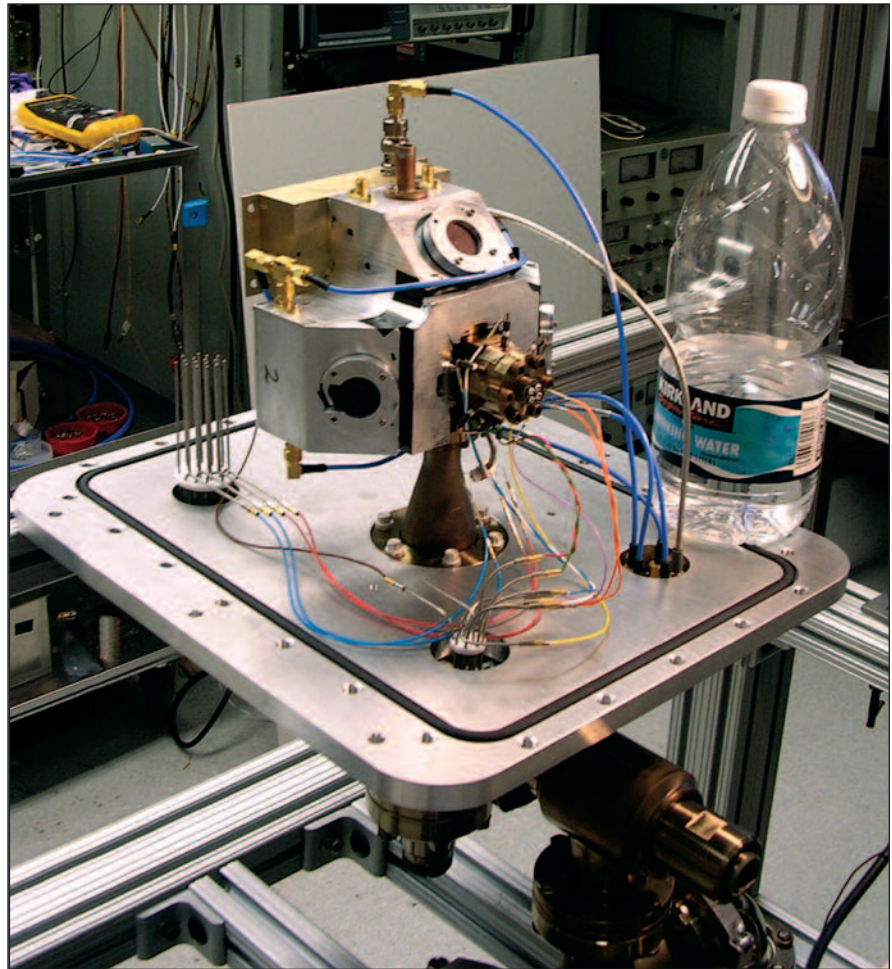
NASA's Jet Propulsion Laboratory, Pasadena, California

A mercury-ion clock now at the breadboard stage of development (see figure) has a stability comparable to that of a hydrogen-maser clock: In tests, the clock exhibited an Allan deviation of between 2×10^{-13} and 3×10^{-13} at a measurement time of 1 second, averaging to about 10^{-15} at 1 day. However, the clock occupies a volume of only about 2 liters — about a hundredth of the volume of a hydrogen-maser clock. The ion-handling parts of the apparatus are housed in a sealed vacuum tube, wherein only a getter pump is used to maintain the vacuum. Hence, this apparatus is a prototype of a generation of small, potentially portable high-precision clocks for diverse ground- and space-based navigation and radio science applications. Furthermore, this new ion-clock technology is about 100 times more stable and precise than the rubidium atomic clocks currently in use in the NAVSTAR GPS Earth-orbiting satellites.

In this clock, mercury ions are shuttled between a quadrupole and a 16-pole linear radio-frequency trap. In the quadrupole trap, the ions are tightly confined and optical state selection from a ^{202}Hg radio-frequency-discharge ultraviolet lamp is carried out. In the 16-pole trap, the ions are more loosely confined and atomic transitions resonant at frequency of about 40.507 GHz are interrogated by use of a microwave beam at that frequency.

The trapping of ions effectively eliminates the frequency pulling caused by wall collisions inherent to gas-cell clocks. The shuttling of the ions between the two traps enables separation of the state-selection process from the clock microwave-resonance process, so that each of these processes can be optimized independently of the other.

The basic ion-shuttling, two-trap scheme as described thus far is not new: it has been the basis of designs of prior larger clocks. The novelty of the present development lies in major redesigns of its physics package (the ion traps and the vacuum and optical sub-



The **Physics Package** of the breadboard liter-sized ion clock is shown here with a connection to an ultrahigh-vacuum pump. The base plate, not part of the package, is used for thermo-vacuum tests of the package. The liter water bottle is shown for scale.

systems) to effect the desired reduction of size to a volume of no more than a couple of liters. The redesign effort has included selection of materials for the vacuum tube, ion trap, and ultraviolet windows that withstand bakeout at a temperature of $\approx 450^\circ\text{C}$ in preparation for sealing the tube to contain the vacuum. This part of the redesign effort follows the approach taken in the development of such other vacuum-tube electronic components as flight traveling-wave-tube amplifiers having operational and shelf lives as long as 15 years.

The redesign effort has also included a thorough study of residual-gas-induced shifts of the ion-clock frequency and a study of alternative gases as candidates for use as a buffer gas within the sealed tube. It has been found that neon is more suitable than is helium, which has been traditionally used for this purpose, in that the pressure-induced frequency pulling by neon is between a third and a half of that of helium. In addition, because neon diffuses through solids much more slowly than does helium, the loss of neon by diffusion over the operational lifetime is expected to be negligible.

The redesign of the optical system has included the formulation of a modular optical-system design that integrates lenses, mirrors, the lamp and its radio-frequency exciter, a photomultiplier tube, and pulse-generation electronic circuitry, into a small package that is attached to the vacuum tube in alignment with the optical ports on the surface of the tube and with the ion trap inside the tube. A reference mag-

netic-field coil, an inner magnetic shield, and a 40.507-GHz microwave feed with window have also been incorporated.

This work was done by John Prestage of Caltech for NASA's Jet Propulsion Laboratory.

In accordance with Public Law 96-517, the contractor has elected to retain title to this invention. Inquiries concerning rights for its commercial use should be addressed to:

Innovative Technology Assets Management
JPL
Mail Stop 202-233
4800 Oak Grove Drive
Pasadena, CA 91109-8099
(818) 354-2240
E-mail: iaoffice@jpl.nasa.gov
Refer to NPO-43075, volume and number of this NASA Tech Briefs issue, and the page number.

LiGa(OTf)₄ as an Electrolyte Salt for Li-Ion Cells

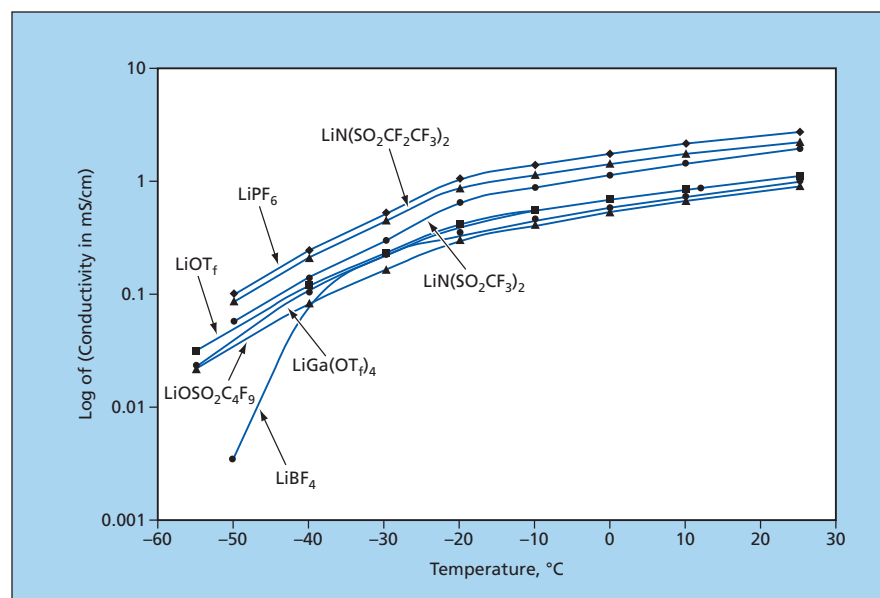
This salt could improve rechargeable lithium-ion cell performance.

NASA's Jet Propulsion Laboratory, Pasadena, California

Lithium tetrakis(trifluoromethanesulfonato)gallate [abbreviated "LiGa(OTf)₄" (wherein "OTf" signifies trifluoromethanesulfonate)] has been found to be promising as an electrolyte salt for incorporation into both liquid and polymer electrolytes in both rechargeable and non-rechargeable lithium-ion electrochemical cells. This and other ingredients have been investigated in continuing research oriented toward improving the performances of rechargeable lithium-ion electrochemical cells, especially at low temperatures.

This research at earlier stages, and the underlying physical and chemical principles, were reported in numerous previous *NASA Tech Briefs* articles. As described in more detail in those articles, lithium-ion cells most commonly contain non-aqueous electrolyte solutions consisting of lithium hexafluorophosphate (LiPF₆) dissolved in mixtures of cyclic and linear alkyl carbonates, including ethylene carbonate (EC), propylene carbonate (PC), dimethyl carbonate (DMC), diethyl carbonate (DEC), and ethyl methyl carbonate (EMC). Although such LiPF₆-based electrolyte solutions are generally highly ionically conductive and electrochemically stable, as needed for good cell performance, there is interest in identifying alternate lithium electrolyte salts that, relative to LiPF₆, are more resilient at high temperature and are less expensive.

Experiments have been performed on LiGa(OTf)₄ as well as on several other candidate lithium salts in pursuit of this interest. As part of these experiments, LiGa(OTf)₄ was synthesized by the reaction of Ga(OTf)₃ with an equimolar portion of LiOTf in a solvent consisting of anhydrous acetonitrile. Evaporation of the solvent yielded



Ionic Conductivities of 0.10 M Solutions of the indicated lithium salts in equal volume parts of PC and DMC were measured at temperatures from -50 to +25 °C. The salts other than LiPF₆, including LiGa(OTf)₄ have been investigated as candidates to supplant LiPF₆.

LiGa(OTf)₄ as a colorless crystalline solid. The LiGa(OTf)₄ and the other salts were incorporated into solutions with PC and DMC. The resulting electrolyte solutions exhibited reasonably high ionic conductivities over a relatively wide temperature range down to -40 °C (see figure). In cyclic voltammetry measurements, LiGa(OTf)₄ and the other salts exhibited acceptably high electrochemical stability over the relatively wide potential window of 0 to 5 V versus Li⁺/Li. ¹³C nuclear-magnetic-resonance measurements yielded results that suggested that in comparison with the other candidate salts, LiGa(OTf)₄ exhibits less ion pairing.

Planned further development will include optimization of the salt and sol-

vent contents of such electrolyte solutions and incorporation of LiGa(OTf)₄ into gel and solid-state polymer electrolytes. Of the salts, LiGa(OTf)₄ is expected to be especially desirable for incorporation into lithium polymer electrolytes, wherein decreased ion pairing is advantageous and the large delocalized anions can exert a plasticizing effect.

This work was done by V. Prakash Reddy of the University of Missouri-Rolla; G.K. Syria Prakash, Jinbo Hu, and Ping Yan of the University of Southern California; and Marshall Smart, Ratnakumar Bugga, Keith Chin, and Subbarao Surampudi of Caltech for NASA's Jet Propulsion Laboratory. For more information, contact iaoffice@jpl.nasa.gov. NPO-41516

Compact Dielectric-Rod White-Light Delay Lines

Achievable group delays would be limited only by optical losses in materials.

NASA's Jet Propulsion Laboratory, Pasadena, California

Optical delay lines of a proposed type would be made from rods of such dielectric materials as calcium fluoride, fused silica, or sapphire. These would offer advantages over prior optical delay lines, as summarized below.

Optical delay lines are key components of opto-electronic microwave oscillators, narrow-band opto-electronic microwave filters, evanescent-field optical biochemical detectors, and some Fourier-Transform spectrum analyzers. Heretofore, optical delay lines used in such applications have been of two types: resonators and coiled long optical fibers, both of which have disadvantages:

- Resonators are compact, but excitation must be provided by narrow-band lasers. Wide-band (including noisy) laser light cannot be coupled efficiently to narrow-band resonators.
- When light is coupled into a narrow-band resonator from a source of reasonably high power, a significant

amount of optical energy circulates within the resonator, causing nonlinear loss and significant noise.

- Typically, a coil-type optical delay line is made of fused-silica fiber, which exhibits fundamental loss. To overcome the limit imposed by the optical loss in fused silica, it would be necessary to use fibers having crystalline cores.
- Although space is saved by winding fibers into coils, fiber-coil delay lines are still inconveniently bulky.

The proposed compact dielectric-rod delay lines would exploit the special class of non-diffracting light beams that are denoted Bessel beams because their amplitudes are proportional to Bessel functions of the radii from their central axes. High-order Bessel beams can have large values of angular momentum. They can be generated with the help of whispering-gallery-mode optical resonators, as described, for example, in "Simplified Generation of High-Angu-

lar-Momentum Light Beams" (NPO-42965) *NASA Tech Briefs*, Vol. 31, No. 3 (March 2007), page 8a. In a delay line according to the proposal, the dielectric rod would be dimensioned to function as a multimode waveguide. Suitably chosen high-angular-momentum modes in such a waveguide exhibit low group velocity (hence, long delay) and no resonance. Such a delay line could perform well at any wavelength or range of wavelengths within the transparency wavelength band of the dielectric material, and the maximum possible group delay achievable through suitable design would be limited only by the optical loss in the rod material.

This work was done by Lute Maleki, Andrey Matsko, Anatoliy Savchenkov, and Dmitry Strelakov of Caltech for NASA's Jet Propulsion Laboratory. Further information is contained in a TSP (see page 1).NPO-43459

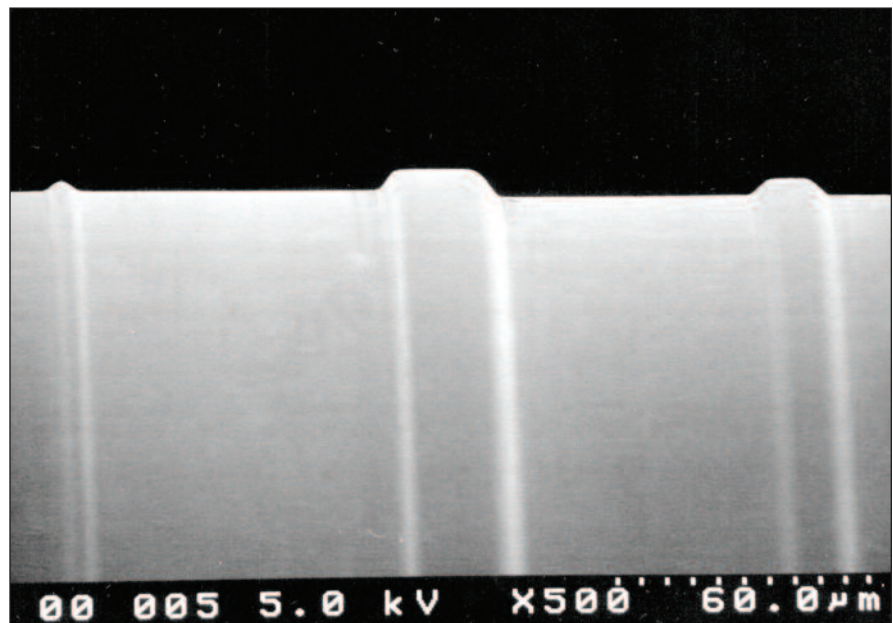
Single-Mode WGM Resonators Fabricated by Diamond Turning

Resonators having desired spectral responses can be reproduced efficiently.

NASA's Jet Propulsion Laboratory, Pasadena, California

A diamond turning process has made possible a significant advance in the art of whispering-gallery-mode (WGM) optical resonators. By use of this process, it is possible to fashion crystalline materials into WGM resonators that have ultra-high resonance quality factors (high Q values), are compact (ranging in size from millimeters down to tens of microns), and support single electromagnetic modes.

This development combines and extends the developments reported in "Few-Mode Whispering-Gallery-Mode Resonators" (NPO-41256), *NASA Tech Briefs*, Vol. 30, No. 1 (January 2006), page 16a and "Fabrication of Submillimeter Axisymmetric Optical Components" (NPO-42056), *NASA Tech Briefs*, Vol. 31, No. 5 (May 2007), page 10a. To recapitulate from the first cited prior article: A WGM resonator of this special type consists of a rod, made of a suitable transparent material, from which protrudes a thin circumferential belt of the same material. The



Circumferential Belts were formed by diamond turning on the initially cylindrical surface of a CaF_2 rod. The radial depths and axial widths of the belts were chosen to make some of the belts act as single-mode and some as multi-mode WGM resonators.

belt is integral with the rest of the rod and acts as a circumferential waveguide. If the depth and width of the belt are made appropriately small, then the belt acts as though it were the core of a single-mode optical fiber: the belt and the rod material adjacent to it support a single, circumferentially propagating mode or family of modes.

To recapitulate from the second cited prior article: A major step in the fabrication of a WGM resonator of this special type is diamond turning or computer numerically controlled machining of a rod of a suitable transparent crystalline material on an ultrahigh-precision lathe. During the rotation of a spindle in which the rod is mounted, a diamond tool is used to cut the rod. A computer program is used to control stepping motors that move the di-

among tool, thereby controlling the shape cut by the tool. Because the shape can be controlled via software, it is possible to choose a shape designed to optimize a resonator spectrum, including, if desired, to limit the resonator to supporting a single mode. After diamond turning, a resonator can be polished to increase its Q .

By virtue of its largely automated, computer-controlled nature, the process is suitable for mass production of nominally identical single-mode WGM resonators. In a demonstration of the capabilities afforded by this development, a number of WGM resonators of various designs were fabricated side by side on the surface of a single CaF_2 rod (see figure).

This work was done by Ivan Grudin, Lute Maleki, Anatoliy Savchenkov, Andrey

Matsko, Dmitry Strelkov, and Vladimir Ilchenko of Caltech for NASA's Jet Propulsion Laboratory. Further information is contained in a TSP (see page 1).

In accordance with Public Law 96-517, the contractor has elected to retain title to this invention. Inquiries concerning rights for its commercial use should be addressed to:

*Innovative Technology Assets Management
JPL*

*Mail Stop 202-233
4800 Oak Grove Drive
Pasadena, CA 91109-8099
(818) 354-2240*

E-mail: iaoffice@jpl.nasa.gov

Refer to NPO-43070, volume and number of this NASA Tech Briefs issue, and the page number.

Mitigating Photon Jitter in Optical PPM Communication

Compensation based partly on photon-arrival statistics would yield gain.

NASA's Jet Propulsion Laboratory, Pasadena, California

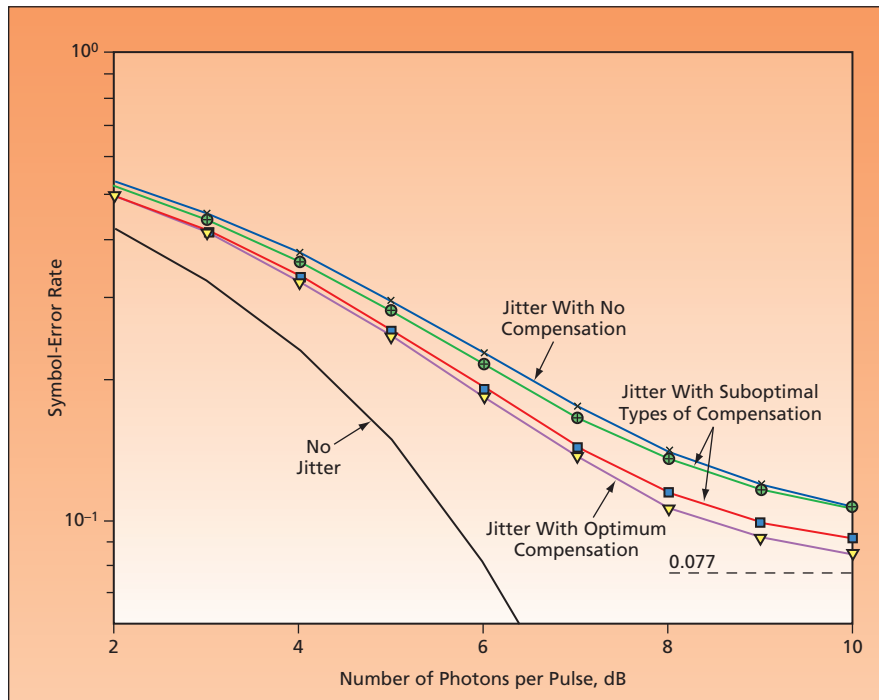
A theoretical analysis of photon-arrival jitter in an optical pulse-position-modulation (PPM) communication channel has been performed, and now constitutes the basis of a methodology

for designing receivers to compensate so that errors attributable to photon-arrival jitter would be minimized or nearly minimized. Photon-arrival jitter is an uncertainty in the estimated time of arrival of

a photon relative to the boundaries of a PPM time slot. Photon-arrival jitter is attributable to two main causes: (1) receiver synchronization error [error in the receiver operation of partitioning time into PPM slots] and (2) random delay between the time of arrival of a photon at a detector and the generation, by the detector circuitry, of a pulse in response to the photon. For channels with sufficiently long time slots, photon-arrival jitter is negligible. However, as durations of PPM time slots are reduced in efforts to increase throughputs of optical PPM communication channels, photon-arrival jitter becomes a significant source of error, leading to significant degradation of performance if not taken into account in design.

For the purpose of the analysis, a receiver was assumed to operate in a photon-starved regime, in which photon counts follow a Poisson distribution. The analysis included derivation of exact equations for symbol likelihoods in the presence of photon-arrival jitter. These equations describe what is well known in the art as a matched filter for a channel containing Gaussian noise. These equations would yield an optimum receiver if they could be implemented in practice.

Because the exact equations may be too complex to implement in practice, approximations that would yield suboptimal receivers were also derived. One



Symbol-Error Rates were computed for a PPM receiver not subject to jitter and for PPM receivers subject to photon-arrival-jitter-induced inter-time-slot interference (neglecting inter-symbol interference), all for the case of 16-time-slot PPM words with an average of 0.2 noise photons per time slot and $\alpha = 0.2$ in a jitter-offset exponential distribution $f(\delta) = [1/(2\alpha)]e^{-\delta/\alpha}$, where δ is the jitter offset in units of one slot duration.

approximation is based on the assumption that the jitter in the arrival of each photon is independent. Another approximation is based on the assumption that only photon counts over finite time bins are available. Yet another approximation is based on the counts-over-finite-time-bins assumption with the addi-

tional assumption that the counts follow a Poisson distribution. For jitter with a standard deviation of 0.28 of a slot, computational-simulation tests have shown that receivers designed to compensate using the exact or approximate equations would exhibit error-rate reductions, relative to receiver designs based

on neglect of photon-arrival jitter, equivalent to power increases of the order of 1 dB (see figure).

*This work was done by Bruce Moision of Caltech for NASA's Jet Propulsion Laboratory. For more information, contact iaoffice@jpl.nasa.gov.
NPO-45163*

MACOS Version 3.31

NASA's Jet Propulsion Laboratory, Pasadena, California

Version 3.31 of Modeling and Analysis for Controlled Optical Systems (MACOS) has been released. MACOS is an easy-to-use computer program for modeling and analyzing the behaviors of a variety of optical systems, including systems that have large, segmented apertures and are aligned with the technology of wavefront sensing and control. Two previous versions were described in "Improved Software for Modeling Controlled Optical Systems" (NPO-19841) *NASA Tech Briefs*, Vol. 21, No. 12 (December 1997), page 42 and "Optics Program Modified for Multithreaded Parallel Computing" (NPO-40572) *NASA Tech Briefs*, Vol. 30, No. 1 (January 2006) page

13a. The present version incorporates the following enhancements over prior versions:

- A powerful system-optimization facility includes algorithms for linear, nonlinear, unconstrained, and constrained optimization of optical systems under a variety of settings.
- There is now enhanced capability to perturb optical components individually and on subsystem levels, and to optimize system performance by adjusting selected individual components as well as subsystems.
- Capabilities for modeling a variety of new optical aperture types have been added.

- Effects of multilayer thin-film coats on optical surfaces can now be taken into account when tracing polarized rays.
- Major software-engineering work was performed to make MACOS more reliable, flexible, and manageable for purposes of maintenance and further development.

This program was written by David Redding, John Lou, Scott Basinger and Norbert Sigrist of Caltech for NASA's Jet Propulsion Laboratory.

This software is available for commercial licensing. Please contact Karina Edmonds of the California Institute of Technology at (626) 395-2322. Refer to NPO-45030.

Fiber-Optic Determination of N₂, O₂, and Fuel Vapor in the Ullage of Liquid-Fuel Tanks

A fiber-optic sensor provides feedback control of onboard inert gas generation systems (OBIGGS) and reduces aircraft operational costs.

John H. Glenn Research Center, Cleveland, Ohio

A fiber-optic sensor system has been developed that can remotely measure the concentration of molecular oxygen (O₂), nitrogen (N₂), hydrocarbon vapor, and other gases (CO₂, CO, H₂O, chlorofluorocarbons, etc.) in the ullage of a liquid-fuel tank. The system provides an accurate and quantitative identification of the above gases with an accuracy of better than 1 percent by volume (for O₂ or N₂) in real-time (5 seconds). In an effort to prevent aircraft fuel tank fires or explosions similar to the tragic TWA Flight 800 explosion in 1996, OBIGGS are currently being developed for large commercial aircraft to prevent dangerous conditions from forming inside fuel tanks by providing an "inerting" gas blanket that is low in oxygen, thus preventing

the ignition of the fuel/air mixture in the ullage.

OBIGGS have been used in military aircraft for many years and are now standard equipment on some newer large commercial aircraft (such as the Boeing 787). Currently, OBIGGS are being developed for retrofitting to existing commercial aircraft fleets in response to pending mandates from the FAA. Most OBIGGS use an air separation module (ASM) that separates O₂ from N₂ to make nitrogen-enriched air from compressed air flow diverted from the engine (bleed air). Current OBIGGS systems do not have a closed-loop feedback control, in part, due to the lack of suitable process sensors that can reliably measure N₂ or O₂ and at the same time, do not constitute an inherent source of ignition.

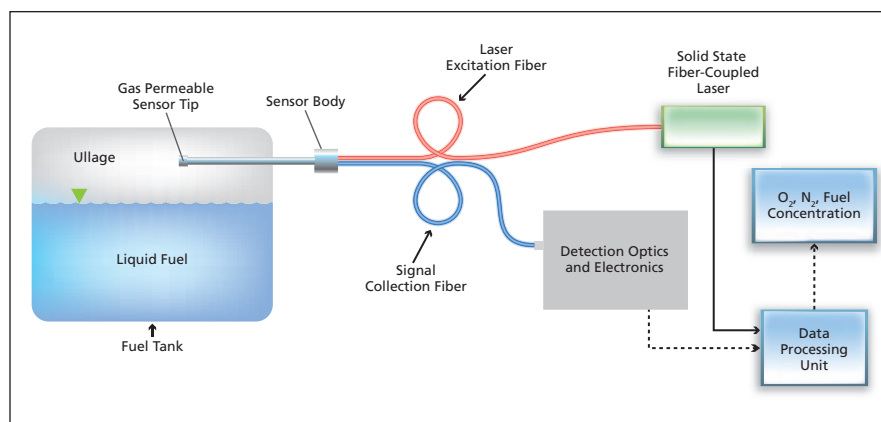
Thus, current OBIGGS operate with a high factor-of-safety dictated by process protocol to ensure adequate fuel-tank inerting. This approach is inherently inefficient as it consumes more engine bleed air than is necessary compared to a closed-loop controlled approach. The reduction of bleed air usage is important as it reduces fuel consumption, which translates to both increased flight range and lower operational costs.

Numerous approaches to developing OBIGGS feedback-control sensors have been under development by many research groups and companies. However, the direct measurement of nitrogen (N₂) is a challenge to most OBIGGS ullage sensors (such as tunable diode laser absorption) as they cannot measure N₂ directly but de-

pend on the measurement of oxygen (O_2). The problem with a singular measure of O_2 , is that as the concentration (number density) of O_2 decreases due to the inerting process or due to lower pressures from high altitudes, the precision and accuracy of the O_2 measurement decreases. However, measuring O_2 density in combination with N_2 density (which is more abundant in air and in a N_2 -inerted fuel tank) can provide a much more accurate and reliable determination of the OBIGGS efficacy.

Perhaps the most important advantage that the present technology has over competing single molecule sensors is the built-in redundancy of the simultaneous O_2 and N_2 measurement, which minimizes the possibility of false high-oxygen OBIGGS alarms, and its impact on airline operational costs that can result from a safety-required takeoff abort or forced-landing. The fiber-optic sensor system described here is inherently reliable as it has no moving parts or sensor materials that wear out or are consumed. Furthermore, the system is compact, lightweight, and requires little power (<20 W) for use aboard aircraft. The sensor technology itself does not present an intrinsic fire or explosion safety hazard compared to electrically based sensors that require wiring, which can serve as ignition sources within a fuel tank.

The present technology provides a fiber-optically-coupled gas sensor head that uses a low power (<30 mW) solid-state laser and optical detection system to yield high signal-to-noise ratios (10^4) of multiple gas densities in a real-time mode. The optical signals from the sensor system are then digitized and processed by a rugged embedded micro-



Schematic of the Fiber-Optic Ullage Oxygen/Nitrogen Sensor System shows the sensor probe head mounted in the fuel tank through a bulkhead fitting. The laser and detection optics and electronics can be mounted remotely from the fuel tank in the avionics compartment. Multiple fiber optics sensor heads (up to 8) can be connected to a common detection optics unit for cost-effective deployment in configurations with multiple fuel tanks or multiple locations within a fuel tank.

controller unit (MCU). The MCU provides quantitative data streams representing the measured species concentration of N_2 , O_2 for active-feedback control, and an alarm signal for aircraft operations.

In operation, the sensor probe head is mounted in the fuel-tank ullage, using a bulkhead flange type mount. The laser and detection optics and electronics can be mounted remotely in the avionics cabinet, away from the harsh environment that surrounds the fuel tank. The remote fiber-optic mounting enhances serviceability and provides system installation flexibility. This flexibility includes the ability for a single detection optics unit to monitor up to eight separate probe heads for a cost-effective deployment. Finally, the present system can also be used to reliably detect fires in inaccessible locations aboard an aircraft (engine nacelle, cabling and hydraulic line compartment, wheel well, and the

like) by detecting low O_2 , with enhanced CO_2 and CO, both by-products of combustion and fires.

As an added benefit, the present technology can also measure the concentration of chlorofluorocarbons (CFC's) that are used to suppress fires to confirm that fire-suppression measures have been properly executed. Such a fire detection system also has the advantage of very low false-alarm rates as multiple chemical species are detected and required to trigger a fire alarm.

This work was done by Quang-Viet Nguyen of Glenn Research Center. Further information is contained in a TSP (see page 1).

Inquiries concerning rights for the commercial use of this invention should be addressed to NASA Glenn Research Center, Innovative Partnerships Office, Attn: Steve Fedor, Mail Stop 4-8, 21000 Brookpark Road, Cleveland, Ohio 44135. Refer to LEW-17826-1.



Spiking Neurons for Analysis of Patterns

High-performance pattern-analysis systems could be implemented as analog VLSI circuits.

NASA's Jet Propulsion Laboratory, Pasadena, California

Artificial neural networks comprising spiking neurons of a novel type have been conceived as improved pattern-analysis and pattern-recognition computational systems. These neurons are represented by a mathematical model denoted the state-variable model (SVM), which among other things, exploits a computational parallelism inherent in spiking-neuron geometry. Networks of SVM neurons offer advantages of speed and computational efficiency, relative to traditional artificial neural networks. The SVM also overcomes some of the limitations of prior spiking-neuron models. There are numerous potential pattern-recognition, tracking, and data-reduction (data preprocessing) applications for these SVM neural networks on Earth and in exploration of remote planets.

Spiking neurons imitate biological neurons more closely than do the neurons of traditional artificial neural networks. A spiking neuron includes a central cell body (soma) surrounded by a treelike interconnection network (dendrites). Spiking neurons are so named because they generate trains of output pulses (spikes) in response to inputs received from sensors or from other neurons. They gain their speed advantage over traditional neural networks by using the timing of individual spikes for

computation, whereas traditional artificial neurons use averages of activity levels over time. Moreover, spiking neurons use the delays inherent in dendritic processing in order to efficiently encode the information content of incoming signals. Because traditional artificial neurons fail to capture this encoding, they have less processing capability, and so it is necessary to use more gates when implementing traditional artificial neurons in electronic circuitry. Such higher-order functions as dynamic tasking are effected by use of pools (collections) of spiking neurons interconnected by spike-transmitting fibers.

The SVM includes adaptive thresholds and submodels of transport of ions (in imitation of such transport in biological neurons). These features enable the neurons to adapt their responses to high-rate inputs from sensors, and to adapt their firing thresholds to mitigate noise or effects of potential sensor failure. The mathematical derivation of the SVM starts from a prior model, known in the art as the point soma model, which captures all of the salient properties of neuronal response while keeping the computational cost low. The point-soma latency time is modified to be an exponentially decaying function of the strength of the applied potential.

Choosing computational efficiency over biological fidelity, the dendrites surrounding a neuron are represented by simplified compartmental submodels and there are no dendritic spines. Updates to the dendritic potential, calcium concentrations and conductances, and potassium-ion conductances are done by use of equations similar to those of the point soma. Diffusion processes in dendrites are modeled by averaging among nearest-neighbor compartments. Inputs to each of the dendritic compartments come from sensors. Alternatively or in addition, when an affected neuron is part of a pool, inputs can come from other spiking neurons.

At present, SVM neural networks are implemented by computational simulation, using algorithms that encode the SVM and its submodels. However, it should be possible to implement these neural networks in hardware: The differential equations for the dendritic and cellular processes in the SVM model of spiking neurons map to equivalent circuits that can be implemented directly in analog very-large-scale integrated (VLSI) circuits.

This work was done by Terrance Huntsberger of Caltech for NASA's Jet Propulsion Laboratory. Further information is contained in a TSP (see page 1). NPO-40945

Symmetric Phase-Only Filtering in Particle-Image Velocimetry

Performance is enhanced significantly with little increase in computation time.

John H. Glenn Research Center, Cleveland, Ohio

Symmetrical phase-only filtering (SPOF) can be exploited to obtain substantial improvements in the results of data processing in particle-image velocimetry (PIV). In comparison with traditional PIV data processing, SPOF PIV data processing yields narrower and larger amplitude correlation peaks, thereby providing more-accurate velocity estimates. The higher signal-to-noise ratios associated with the higher amplitude correlation peaks afford greater robust-

ness and reliability of processing. SPOF also affords superior performance in the presence of surface flare light and/or background light. SPOF algorithms can readily be incorporated into pre-existing algorithms used to process digitized image data in PIV, without significantly increasing processing times.

A summary of PIV and traditional PIV data processing is prerequisite to a meaningful description of SPOF PIV processing. In PIV, a pulsed laser is used to illuminate

a substantially planar region of a flowing fluid in which particles are entrained. An electronic camera records digital images of the particles at two instants of time. The components of velocity of the fluid in the illuminated plane can be obtained by determining the displacements of particles between the two illumination pulses.

The objective in PIV data processing is to compute the particle displacements from the digital image data. In traditional PIV data processing, to which the

present innovation applies, the two images are divided into a grid of subregions and the displacements determined from cross-correlations between the corresponding sub-regions in the first and second images. The cross-correlation process begins with the calculation of the Fourier transforms (or fast Fourier transforms) of the subregion portions of the images. The Fourier transforms from the corresponding subregions are multiplied, and this product is inverse Fourier transformed, yielding the cross-correlation intensity distribution.

The average displacement of the particles across a subregion results in a displacement of the correlation peak from the center of the correlation plane. The velocity is then computed from the displacement of the correlation peak and the time between the recording of the two images. The process as described thus far is performed for all the subregions. The resulting set of velocities in grid cells amounts to a velocity vector map of the flow field recorded on the image plane.

In traditional PIV processing, surface flare light and bright background light give rise to a large, broad correlation peak, at the center of the correlation

plane, that can overwhelm the true particle-displacement correlation peak. This has made it necessary to resort to tedious image-masking and background-subtraction procedures to recover the relatively small amplitude particle-displacement correlation peak.

SPOF is a variant of phase-only filtering (POF), which, in turn, is a variant of matched spatial filtering (MSF). In MSF, one projects a first image (denoted the input image) onto a second image (denoted the filter) as part of a computation to determine how much and what part of the filter is present in the input image. MSF is equivalent to cross-correlation. In POF, the frequency-domain content of the MSF filter is modified to produce a unit-amplitude (phase-only) object. POF is implemented by normalizing the Fourier transform of the filter by its magnitude. The advantage of POFs is that they yield correlation peaks that are sharper and have higher signal-to-noise ratios than those obtained through traditional MSF. In the SPOF, these benefits of POF can be extended to PIV data processing. The SPOF yields even better performance than the POF approach, which is uniquely applicable to PIV type image data.

In SPOF as now applied to PIV data processing, a subregion of the first image is treated as the input image and the corresponding subregion of the second image is treated as the filter. The Fourier transforms from both the first- and second-image subregions are normalized by the square roots of their respective magnitudes. This scheme yields optimal performance because the amounts of normalization applied to the spatial-frequency contents of the input and filter scenes are just enough to enhance their high-spatial-frequency contents while reducing their spurious low-spatial-frequency content. As a result, in SPOF PIV processing, particle-displacement correlation peaks can readily be detected above spurious background peaks, without need for masking or background subtraction.

This work was done by Mark P. Wernet of Glenn Research Center. Further information is contained in a TSP (see page 1).

Inquiries concerning rights for the commercial use of this invention should be addressed to NASA Glenn Research Center, Innovative Partnerships Office, Attn: Steve Fedor, Mail Stop 4-8, 21000 Brookpark Road, Cleveland, Ohio 44135. Refer to LEW-17810-1.



Books & Reports

Efficient Coupler for a Bessel Beam Dispersive Element

A document discusses overcoming efficient optical coupling to high orbital momentum modes by slightly bending the taper dispersive element. This little shape distortion is not enough to scramble the modes, but it allows the use of regular, free-beam prism coupling, fiber coupling, or planar fiber on-chip coupling with, ultimately, 100 percent efficiency.

The Bessel-beam waveguide is bent near the contact with the coupler, or a curved coupler is used. In this case, every Bessel-beam mode can be successfully coupled to a collimated Gaussian beam. Recently developed Bessel-beam waveguides allow long optical delay and very high dispersion. Delay values may vary from nanoseconds to microseconds, and dispersion promises to be at 100 $\mu\text{s}/\text{nm}$. Optical setup consisted of a red laser, an anamorphic prism pair, two prism couplers, and a bent, single-mode fiber attached to prisms. The coupling rate in-

creased substantially and corresponded to the value determined by the anamorphic prism pair.

This work was done by Anatoliy Savchenkov, Vladimir Ilchenko, Andrey Matsko, Thanh Le, Nan Yu, and Lute Maleki of Caltech for NASA's Jet Propulsion Laboratory. Further information is contained in a TSP (see page 1). NPO-45440

Attitude and Translation Control of a Solar Sail Vehicle

A report discusses the ability to control the attitude and translation degrees-of-freedom of a solar sail vehicle by changing its center of gravity. A movement of the spacecraft's center of mass causes solar-pressure force to apply a torque to the vehicle. At the compact core of the solar-sail vehicle lies the spacecraft bus which is a large fraction of the total vehicle mass. In this concept, the bus is attached to the spacecraft by two single degree-of-freedom linear tracks. This allows relative movement of the bus in the sail plane. At the null position, the resulting solar pres-

sure applies no torque to the vehicle. But any deviation of the bus from the null creates an offset between the spacecraft center of mass and center of solar radiation pressure, resulting in a solar-pressure torque on the vehicle which changes the vehicle attitude. Two of the three vehicle degrees of freedom can be actively controlled in this manner. The third, the roll about the sunline, requires a low-authority vane/propulsive subsystem.

Translation control of the vehicle is achieved by directing the solar-pressure-induced force in the proper inertial direction. This requires attitude control. Attitude and translation degrees-of-freedom are therefore coupled. A guidance law is proposed, which allows the vehicle to stationkeep at an appropriate point on the inertially-rotating Sun-Earth line. Power requirements for moving the bus are minimal. Extensive software simulations have been performed to demonstrate the feasibility of this concept.

This work was done by Gurkirpal Singh of Caltech for NASA's Jet Propulsion Laboratory. Further information is contained in a TSP (see page 1). NPO-44129



National Aeronautics and
Space Administration